Dissertation:

Analysis Methods in Wood and Natural Fibre Science

Applying Nanoindenter and Atomic Force Microscope

Universität für Bodenkultur Wien

Department for Material Sciences and Process Engineering

Institute of Wood Technology and Renewable Materials

Head of Institute: Wolfgang GINDL-ALTMUTTER

Advisor: Wolfgang GINDL-ALTMUTTER

ANALYSIS METHODS IN WOOD AND NATURAL FIBRE SCIENCE APPLYING NANOINDENTER AND ATOMIC FORCE MICROSCOPE

Dissertation
for obtaining a doctorate degree
at the University of Natural Resources and Applied Life Sciences Vienna

Submitted by
Michael OBERSRIEBNIG

Vienna, October 2014

This Work Is Dedicated To My Parents.

Thank You For All The Strength And Support.

Acknowledgements

I want to thank at this point the many people who helped me in writing and finishing this doctoral thesis, a few of which shall be mentioned specifically. First and foremost, I want to thank my supervisor Prof. Wolfgang Gindl-Altmutter for the chance and the support to write this thesis. Prof. Johannes Konnerth and my colleague Dr. Stefan Veigl I want to give thanks for all the advice and discussions and their general helpfulness with any questions and problems I had. Special thanks also to our institute technician Gerhard Emsenhuber who helped me out with any technical difficulties. Not unmentioned should go my friends, whose support gave me strength and who willingly listened to any complaints and ramblings. A very big thanks here to Eva Lems for all the kilometres on the running tracks around Vienna and hours on climbing walls. Finally, and definitely not the least, I want to thank my family and especially my parents. Thank you for always supporting me, providing a safe haven when needed and the wings to fly out into the world.

Zusammenfassung

Das Ziel dieser Doktorarbeit war die Entwicklung und Implementierung neuer Methoden zur Mikro- und Nanocharakterisierung im Bereich der Naturfaserforschung. Als Instrumente standen hierbei speziell Nanoindenter und Rasterkraftmikroskop zur Verfügung. In Paper 1 wird eine neue Methode zur Adhäsionsmessung mittels Nanoindenter direkt an der Grenzfläche zwischen Zellwand und Leim präsentiert. Diese Methode wird in Paper 2 angewendet, um Unterschiede im Adhäsionsverhalten zweier Leimtypen an der S2- und S3-Zellwandschicht von Fichtenholz zu untersuchen. Der Zusammenhang zwischen Nanorauheit gemessen mit dem Rasterkraftmikroskop und dem optischen Erscheinen von Lignozelluloseoberflächen wird in Paper 3 undersucht. Paper 4 untersucht zeitabhängige Änderungen der Oberflächenchemie der S2- und S3-Schicht der Holzzellwand mittels Kraftscans. In Paper 5 wird die richtungsabhängige Wärmeleitfähigkeit von Holzproben mittels Scanning Thermal Microscopy untersucht. Weitere Arbeiten an dieser Methode mit dem Ziel einer quantitativen Messung werden im Experimentalteil der Arbeit präsentiert.

Abstract

The aim of this doctoral thesis was the development and implementation of new methods for micro- and nano-characterisation in natural fibre science. The main experimental devices for this were nanoindenter and atomic force microscope. A new method for measuring the cell wall-adhesive interaction directly at the interface by means of nanoindentation is presented in Paper 1. This method is applied in Paper 2 to analyse differences in the bonding behaviour of two types of adhesives to the S2 and S3 cell wall, respectively, of spruce wood. Measuring nanoscale roughness with the AFM, Paper 3 investigates the influence of roughness on the optical appearance of ligno-cellulosic fibres. Paper 4 examines temporal changes in surface chemistry of the S2- and S3 cell wall layer by applying a mechanical mapping mode. Paper 5 introduces scanning thermal microscopy to evaluate the direction-dependent thermal conductivity of wood samples on the cell wall level. Further work on this method with the aim of obtaining quantitative results for fibrous materials is presented in the experimental section of this thesis.

Contents

List of Abbreviations

AFM - atomic force microscope, atomic force microscopy

CC - conductivity contrast

CS-NI - cross-sectional nanoindentation

EM - electron microscope, electron microscopy

NI - nanoindenter, nanoindentation

PUR - polyurethane

QNM - quantitative nanomechanical mapping

UF - urea formaldehyde

SThM - scanning thermal microscopy

TC - thermal conductivity

Introduction

Wood has for centuries been the single most important raw material in large parts of the world and still is, as production numbers show [1]. As such, its properties are very well analysed and discribed on a macroscopic scale in all its different varieties, as several comprehensive publications stand to prove (e.g. [2, 3][3]). On the microscopic scale, however, there is still only limited knowledge available. To a large part this is due to a lack of methods in this regime. This becomes even more of a let-down, as with the increased use of particle boards, wood particle based composites and nanocellulose composites it becomes more important to obtain knowledge about material behaviour on the micro- and nanoscale. The aim of this work, therefore, was to introduce and improve methods in this regime to natural material science. The main experimental equipment used during this work were a triboindenter used in collaboration with the Technical University Vienna, and an atomic force microscope (AFM) available at the Institute of Wood Technology and Renewable Materials, BOKU Vienna, where the main part of work for this thesis was conducted.

The first two articles focus on nanoindentation (NI) methods. NI is a means of investigating the mechanical properties of materials similar to conventional indentation tests like the Rockwell test, with simultaneous force and depth sensing. Its very high spatial resolution makes it especially suitable for thin films and materials showing heterogeneity below the mm range, where standard deformation testing methods are

too crude. The low size of the indents however prevents the optical analysis of the residual indents and demands for more sophisticated approach. A very good overview over the principles and problems of NI measurements is given in by Oliver and Pharr in their reviews ([4] and [5]). Wimmer et al. [6] were the first to introduce NI to wood science. By now it is established as standard method in this field, as various articles stand to prove (e.g. [7, 8, 9, 10]). A lot of research also goes into refining the method specifically for applications on wood (e.g. [11, 12, 13]).

Sanchez et al. ([14]) introduced an unconventional new approach to allow evaluation of the specific energy of adhesion of thin films by NI. They performed measurements of work of indentation on the cross section of an adhesively bonded thin metal bi-layer on a silica surface, an important bond type in integrated circuit design. Combining their results with computational models of the crack building and material deformation processes, they were able to derive the specific energy of adhesion. This approach was further refined and successfully applied by Elizalde et al. ([15]). These works served as inspiration to try a similar approach for wood, modified for the different material behaviour of the wooden cell wall and wood adhesives, to gain information about adhesion energy on the wood cell wall level. This method is introduced and tested on surface modified wood samples in Paper 1. Paper 2 applies this technique to show for an urea formaldehyde (UF) and a polyurethane (PUR) bonded system, respectively, fundamental differences in bonding behaviour between the S2 and S3 cell wall section.

The further articles apply various modes of measurement of the AFM. AFM is a form of scanning probe microscopy, in which a probe fastened to a lever is scanned across the surface of interest. Direct force interactions between scanning probe and surface not only allow to get a high resolution image of the surface, but also to investigate various physical properties of the sample. This fact combined with its considerable ease of use have made AFM an important device in material science since being introduced by

Binnig and Rohrer in 1986 [16]. A number of articles focussing on AFM investigation of a wide range of properties serve to show the importance of the AFM in natural fibre science (e.g. [17, 18, 19, 20, 21, 22, 23]), with a considerably bigger number where AFM is used as supportive method. In relation to other methods, AFM is still only a minor scientific tool in this field, though. The work done in the course of this thesis is supposed to strengthen its position as research device, by applying new applications and demonstrating its versatility as method in general.

The most principle use of AFM, imaging of surface topography, is applied in Paper 3. De la Rie [24] has shown for paintings that surface roughness is an influencing factor on colour saturation and gloss. That this stands true even for roughness on the nanometre scale as measured by AFM was shown by Watanabe et al. on hair [25]. While wood coatings and appearance are a very important field in wood science, so far this topic remained uninvestigated for wood surfaces. By evaluating the surface roughness from AFM topography images with colour measurements and surface chemical analysis, this article therefore tries to evaluate the influence of surface structure on the appearance of wood.

Another key strength of the AFM is the possibility to measure minute forces on the nanometre scale. Force modes on the AFM all follow the same principle, outlined e.g. by Noy et al. [26] and Butt et al. [27]. In short, a small load-displacement curve is collected on the surface and evaluated in terms of tip-sample adhesion or sample surface mechanics. In wood and natural fibre science, a number of articles on chemical force microscopy have been published [28, 29, 30, 31]. In paper 4, a rather new force mode, called Quantitative Nanomechanical Mapping (QNM), is applied to evaluate temporal changes in the tip-surface adhesion on freshly cut wood surfaces. The main advantage of this mode in comparison to previous force modes is the comparatively high scanning speed while still being able to obtain quantitative results.

Still another method is scanning thermal microscopy (SThM). It allows to investigate thermal properties with a resolution <100nm, limited by the tip radius of thermally conductive probes. On the macroscopic level, thermal properties of wood and as such thermal conductivity (TC) are already quite well researched and documented (e.g. [32, 33, 34]). Little data is available however as to how it follows from the properties of the cell wall components and wood superstructure. A few publications doing computational models exist [35, 36, 37], but no experimental data whatsoever. Developing a working AFM-based method to probe thermal properties on the cell wall level and below could help provide this data. The work presented in Paper 5 could act as a first step in this direction, applying SThM on different wood samples in their principle anatomical directions. Further not yet published work on this method is included at the end of the experimental section

Published Articles

Materials and Methods

Materials

All nanoindentation experiments (Paper 1 and 2) were performed on spruce (Picea abies) wood samples. The adhesives used were a commercially available urea formaldehyde adhesive (Paper 1 and 2) and a commercially available polyurethane adhesive (Paper 2). To provide a model system of samples with stepwise increased hydrophobicity, samples for Paper 1 were subjected to various silane treatments (γ - aminopropyltriethoxysilane, dichlorodiphenyl- silane, octadecyltrichlorosilane and chlorotrimethylsilane).

The oils used in Paper 3 were commercially available walnut oil, linseed oil, sunflower oil and castor oil. Typha fibres (Typha latifolia) were used as nanocellulosic fibres for AFM measurements, as wood thin sections proved impractical due to the cell cavities.

Experiments presented in Paper 4 were conducted on longitudinal sections of spruce (Picea abies) and beech (Fagus sylvatica) samples.

TC measurements in Paper 5 were performed on spruce wood (Picea abies), beech wood (Fagus sylvatica) and oak wood (Quercus robur) samples, respectively.

Methods

Cross-sectional Nanoindentation

Cross-sectional nanoindentation (CS-NI) was first introduced by Sanchez et al. [14], utilizing NI to measure adhesive strength of a thin metal bilayer bonded to a silica bulk. By applying a load onto the silica close to the interface, the brittle silica cracks under stress, with the crack paths directed towards and then following the weakest interface. This approach was taken as motivation to try a modified method on wood. The modifications had to account for the different material behaviour of wood and wood adhesives, i.e. plastic deformation under load rather than crack propagation. Two main modifications were necessary, therefore (Figure 1). First, the indent position was switched from close to the interface directly to the interface. Second, instead of using a Berkovich type tip (a rather flat indenter tip in the shape of a three-sided pyramid which is standard for material tests), a sharp, cone-shaped indenter tip with a total opening angle of 60° and a nominal tip radius of 100nm was used. The sharpness is necessary to allow for deep indents to provide enough delamination even without crack formation. The radial symmetry of the cone (in contrast to e.g. a pyramid) accounts for the heterogeneity and orientation in the wood cell wall. Konnerth et al. [38] have shown for hardness measurements with a Berkovich indenter tip, that results deviate depending on the indent position along the cell wall, due to variations in the relative orientation of microfibrils to the indenter axis. By choosing a rotary symmetric tip, the relative position along the cell wall is non-relevant as long as the microfibril angle is constant and the indenter axis parallel to the cell axis. In sample preparation, special care has to be taken therefore to provide an optimal orientation of the sample.

Generally, the sample preparation closely follows the steps described by Konnerth et

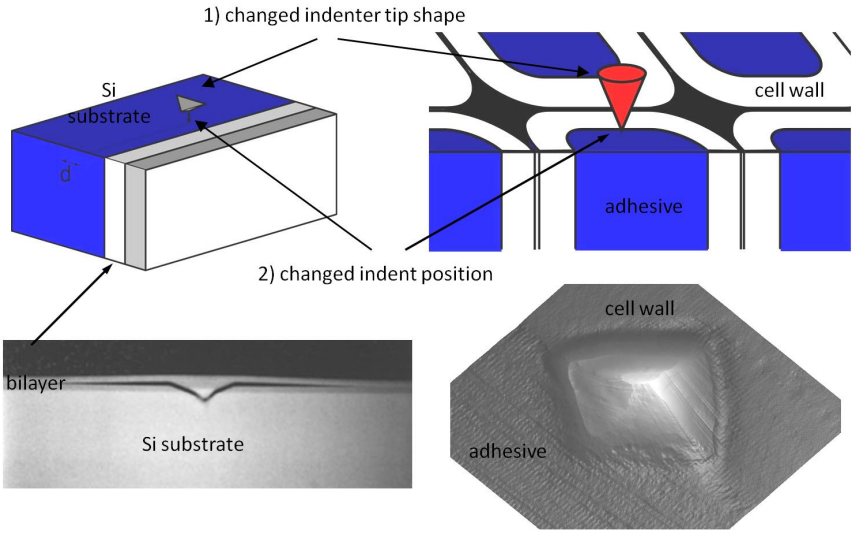

Figure 1: Schematic of original experimental set-up and modified version for wood adhesion, with electron microscopy (EM, original) and AFM image (wood) of the tested sample below. To account for different material properties of the wood cell wall and wood adhesives, the indent position is switched from the bulk to the bond line, and instead of a flat Berkovich type tip a cone-shaped tip is utilized. In the EM image, the crack path is clearly visibly. The total image size is 60µm. No crack formation is visible in the AFM image on a wood-urea formaldehyde sample (total image size is 2µm). The EM image is taken from the original paper by Sanchez et al. [14]

al. **[39]**. Embedding the sample in epoxy can usually be omitted as long as the adhesive bond is strong enough to prevent sample damage during preparation. The indentation and analysis process can be outlined by the following steps:

nanoindentation

- preselecting suitable positions on light micrographs (Figure2a)
- approaching position and scan with nanoindenter tip acting as scanning probe
- choose exact indent position via the SPM-image exactly at cell wall - adhesive interface (Figure 2b)
- perform indent

data analysis

- calculate work of indentation as integral of the force displacement curve
- statistical analysis

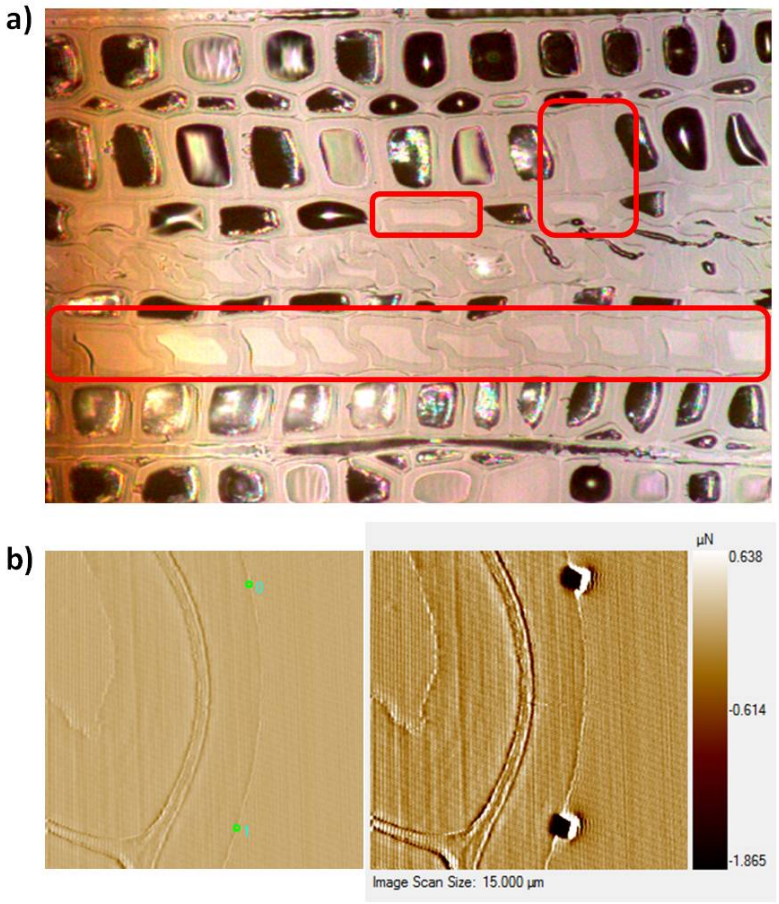

Figure 2: a) Light micrograph for pre-selection of possible indent positions (red frames); b) 15µm-scans taken with the indenter for positioning of indents before (left) and for control after the test (right)

Atomic Force Microscopy - Topography

The ability to create high resolution topography images on literally any surface is the most common application of the AFM. The biggest advantages of AFM imaging as

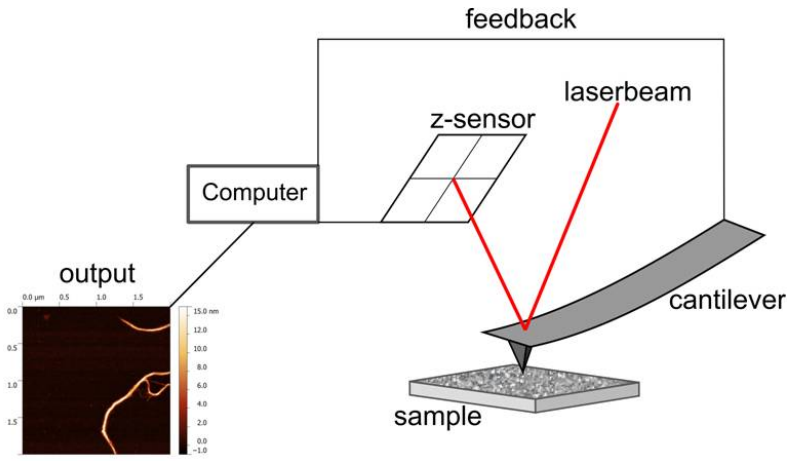

Figure 3: Schematic illustration of AFM principle. The cantilever with the tip scans across the surface. A sensor (now commonly a laser beam light lever) detects the z-movement. This data is transmitted to the computer. There, a topographical map of the surface is created and depicted on the monitor while the z-corrections are sent as feedback signal to the z-Piezzo.

compared to EM is the ability to image non-conductive samples, the possibility to work at varying climates and in fluids and the easy sample preparation, as mostly all that is needed is a smooth enough sample surface.

The basic idea is as simple as it is ingenious and did not change much since its first introduction in 1986 [16]. A sharp tip, fastened to a flexible cantilever with its movement controlled by a Piezzo crystal is scanning across the surface of interest. A sensor collects data on the tip's z-position at every image point. This data is translated to a binary signal which is then depicted as 2D colour-coded image on the monitor. Optionally, a feedback-cycle adjusts the Piezzo crystal according to the sensed tip displacement, thus keeping a constant force on the tip (Figure 3). The most common z-position sensor method now is the light lever. Here, a laser beam is reflected from the back of the cantilever towards a sensor field. When the cantilever is moved from its neutral position, the reflected beam changes position and will either give a positive or negative signal. The feedback cycle changes z-position until the cantilever is in

neutral position again, and collects the feedback data as z information.

For measurements in Paper 3, tapping mode or intermittent contact mode imaging was used. In this mode, the cantilever is set to vibrate close to its Eigen frequency, usually in the range of 100-500kHz. Tip-sample contact is only made at the lower amplitude peak. Varying the peak amplitude and amplitude setpoint allows to decide whether to work in the repulsing force regime, where the tip effectively stops above the sample surface, or in the attractive force regime and make actual surface contact. Working in the repulsive regime has the advantage of prohibiting tip or sample damage on the cost of losing resolution. With an increased tip-sample force, it is the other way round when the tip will actually touch the surface. Compared to contact mode imaging, both modes are slightly slower. However, the non-existence of shear forces lowers risk of damage and can increase image quality.

Atomic Force Microscopy - QNM

QNM mode allows to investigate physical and chemical properties of the sample surface which can be derived from contact force interactions of tip and sample. In contrast to tapping mode imaging, where the cantilever is excited close to its Eigen frequency, here the vibration follows a pulsed sinusoidal pattern with a frequency of about 1-2kHz. This rather low frequency is necessary to allow at every tip-sample contact to perform a minute indent, collecting a force-displacement curve. These curves are evaluated on line to give maps of the surface elastic modulus, the tip-sample adhesion and the energy dissipation in addition to the topography image. Depending on the sample, the adhesion channel and the modulus and dissipation channel often mutually exclude each other due to the measurement principle. To obtain data on the modulus, an indent depth of 2-10nm is necessary. Depending on the expected values of modulus, a cantilever with a corresponding spring constant needs to be chosen. A too soft

cantilever will not provide the necessary deformation to obtain data, while a too stiff cantilever basically deforms the whole sample the same, not providing information on any variations within the sample. Measuring the tip-sample adhesion always needs a very soft cantilever on the other hand, as the forces at work are very low. When setting up such an experiment it is therefore usually necessary to focus on one magnitude and for modulus measurements to have a rough estimate of the expected values.

To obtain quantitative data, the cantilever needs to be properly calibrated. First, the deflection sensitivity is calibrated by evaluating the linear-elastic segment of a force-displacement curve taken on a non-deformable material. Depending on the cantilever stiffness, this can either be fused silica or a sapphire platelet. Next, the spring constant needs to be calibrated. This is rather simple for soft cantilevers ($k < 0.5N/m$), where it can be derived from the cantilever's thermal vibration pattern. For stiffer cantilevers however, this method is often rather imprecise. Several methods are introduced in the literature (e.g. [40, 41]), but non has so far become a standard procedure. For measurement of mechanical properties (as opposed to adhesion only), same as for NI material tests, the tip sample contact area has to be calibrated. The simple suggested method by the manufacturer for this is performing indents on materials of known modulus and, approximating the tip as a half-sphere, estimate the tip radius from this. Other possibilities are imaging the tip by EM or imaging a characterisation sample and derive the tip shape from the tip-image convolution [42]. Both these methods however are prone to damaging or destroying the tip and can suffer strong inaccuracies [43].

Atomic Force Microscopy - Scanning Thermal Microscopy

In SThM, a thermally conductive probe is used to evaluate surface temperature distribution or TC, depending on the settings. The measurement schematics are depicted

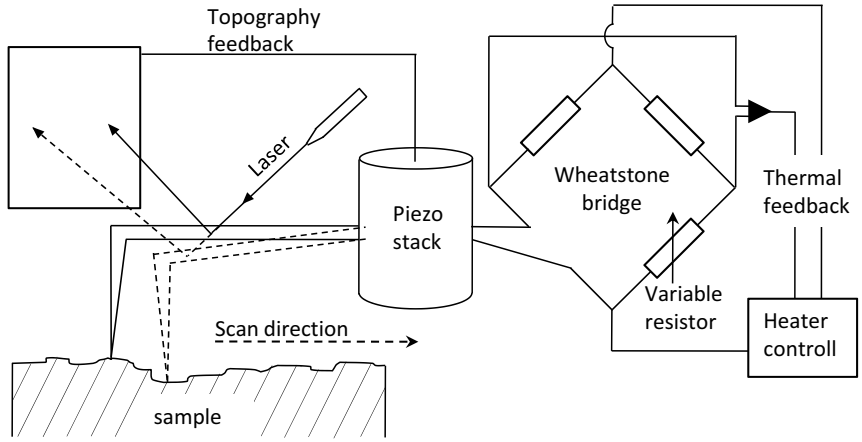

Figure 4: Principle of SThM-measurement. The heated tip constitutes one resistor of a Wheatstone-bridge. Changes in tip temperature cause the resistance to change, thus a non-zero voltage between the branches is measured. This is sent as output signal to the computer. Depending on the current set-up and tip temperature, either sample temperature or TC can be measured.

in Figure 4. The electrically heated tip constitutes one resistor in a Wheatstone bridge. At the start of the measurement, a heating voltage is applied and the bridge voltage is set to zero. A change in temperature of the scanning probe now leads to a change in resistance. As the other elements of the bridge remain constant, the bridge is now out of balance and a non-zero voltage is measured. This can be correlated to a probe temperature change.

Depending on the setup, two different magnitudes can be measured. With the heating voltage low, the probe itself is at a rather low temperature and will take up heat from the sample, thus acting as a nanoscale thermometer. If on the other hand the heating voltage is chosen very high, heat will be transmitted from the probe to the sample. Samples with a high TC will transmit more heat from the probe. Thus, the change in probe temperature and resulting bridge voltage will be correlated to the sample TC. This method was successfully applied in the field of wood science as an indication of glue distribution by Konnerth et al. **[39]**.

The difficulty now lies in obtaining quantitative results. For temperature measurements, this would be quite simple by calibrating the probe with samples of well known temperature, e.g. resistive or Peltier heater elements. For the TC, things are more complicated. Where a periodic heat function is available, the 3-ω- method can be applied [44, 45]. Very briefly put, it derives the TC from the third order harmonic of the heat function period occurring in the heat transmittance function. The disadvantage of this method is that it is math-intensive and not a full-scan method but gets evaluated on selected positions. A different method was suggested by Gomès et al. [46] to analyse nanoporous thin films. By analysing films of same thickness, they were able to obtain a bridge voltage-TC calibration curve and derive quantitative results for their films. This method proved infeasible for wood or natural fibres, however, as thin sections of embedded material could not reliably be brought into full contact with a carrier plate and as such be comparable to the calibration standards. A different approach was therefore to calibrate and test fibres in their longitudinal direction embedded in epoxy. Due to several problems this approach did not reach further than the stage of a pre-experiment, which will be outlined in a short experimental section below.

Results and Discussion

Experiments conducted for Paper 1 focussed on developing and implementing a new method for adhesion measurement. To this ends, a set of calibration samples with increasingly hydrophobic surface properties but no bulk mechanical changes was produced using chemical surface modification. The effectiveness of the surface treatments was evaluated by contact angle measurements using the sessile drop method [47] and by shear-testing of adhesively bonded samples. The contact angle measurements

showed good wettability for the untreated sample and increasingly polar properties for the various treatments. This result was mirrored by the shear test results, showing good adhesion and wood failure on the untreated reference sample, and stepwise decreased shear strengths for the surface modified samples, with near-zero adhesion strength for the most effective treatment. The CS-NI tests reproduced those trends, with a maximum decrease in mean work of indentation on the S3-adhesive interface by 15% between the reference sample type and the most effectively treated sample type. This difference can be directly attributed to the quality of the adhesive bond, as all other mechanical parameters remained constant. Thus, CS-NI was shown to be a feasibly method for evaluating the quality of adhesive bonds between wood cell wall and adhesive at a prior unavailable resolution.

The method was implemented in Paper 2 to evaluate possible differences in bond quality between the inner S2 and the S3 cell wall layer. To provide smooth S2 interfaces, the sample surfaces were microtomed in a wet state and then let dry prior to bonding. A commercially available UF-adhesive and a PUR-adhesive were chosen to represent two of the most common wood adhesive systems with varying properties (UF as polar system, PUR as rather unpolar system). After drying to standard climate, the samples were bonded according to manufacturer specifications. CS-NI results normalized on the S3-adhesive interface results showed a 10% increase of work of indentation on the S2-adhesive interface for the UF-bonded sample, while for the PUR-bonded sample the work of indentation decreased by 5% on the S2-adhesive interface. The increase for the UF system is especially notable in aspect of the results from Paper 1, where the difference in work of indentation between standard adhesion on the S3 and near-0 adhesion was 15%, indicating the strong actual difference in adhesion quality. Analysis of the residual indents with the AFM showed delamination on the PUR-cell wall interface, while no such effect was visible on the UF system.

This might be due to lower adhesion forces as well as the different behaviour of the adhesives. While UF penetrates the cell wall this does not occur for the longer PUR chains. A noteworthy aspect not fully highlighted in the paper is the fact that, due to the necessary preparation steps, the S2 surface was not fresh but already several days old at the time of bonding. As shown in Paper 4 and discussed below, this leads to a significant decrease in surface polarity. Thus, the differences between S2 and S3 cell wall-adhesive interfaces should be even stronger for both adhesives in their respective directions.

The influence of surface roughness on the optical appearance of fibre surfaces was investigated in Paper 3. Different plant oils and UV-radiation were used to modify surface roughness. The roughness was investigated by tapping mode AFM. Chemical surface analysis was done to account for optical changes due to changes in surface chemistry. Evaluation of the data showed a strong positive correlation of roughness and brightness for oil-coated and UV-treated samples. This can be seen as a clear indication of the influence of nanoscale surface roughness. At the same time, however, the UV treated samples showed changes in surface chemistry which could contribute to the change while for the oil-coated samples an influence of the fibre surface-oil interaction could not be discarded. Therefore, no quantification of the effect was given at this time.

Paper 4 made use of the force-sensing capabilities of the AFM to evaluate changes of the surface chemistry of a freshly cut wood cell wall over time. Specific regions containing the S2 and S3 cell wall layer were scanned repeatedly over the course of a week. Statistical analysis of the results on the respective cell wall regions in the adhesion force image provides information on changes in surface polarity. While the S3 layer shows a very slight linear decrease over time which might be due to tip wear, this is not true for the cut-open S2 regions. Those show an exponential decrease in tip-

sample interaction, with the biggest change occurring in the first 24 hours, indicating a decrease in surface hydrophilicity. After this time interval, the adhesion-force curve runs mostly parallel with the linear tip-S3 adhesion force curve, though at a slightly higher force. These results indicate that the known macroscopic effect of wood ageing is mostly due to changes on the fresh cut S2 layers, while the S3 layer remains mostly constant. In aspect of the results of Paper 2, this underlines the known importance of a fresh surface for adhesive wood bonding with rather polar adhesives like UF or MUF adhesives. However, this is not true for more unpolar or amphiphilic adhesives, where longer rest-times before bonding might actually give improved interaction and thus bond quality.

Analysis of micro-TC in the primary wood anatomical directions by SThM was the focus of Paper 5. Measurements were conducted on small, precisely cut wood cubes of of various wood types (spruce, beech and oak) in the longitudinal, radial and tangential direction. Normalizing the results on one arbitrarily chosen and repeatedly scanned position on the longitudinal oak sample allowed cross referencing the results. Results show moderate variations ($\sim$0.1V output voltage) for all scans between the middle lamella and the S2 cell wall layer, with higher values on the S2. This difference is most pronounced in the longitudinal direction, which can be explained by the preferential orientation of microfibrils parallel to the longitudinal axis. However, those slight differences are dwarfed by the strong difference in TC between longitudinal and transversal directions (0.5-0.7V output voltage). While such behaviour could be expected for the S2 layer due to microfibril orientation, the middle lamella was expected to show isotropic or mostly isotropic behaviour. It was argued, therefore, that the high contrast is really due to a factual macroscopic measurement, i.e. the thermal conductance happens over more than just one cell layer. Thus, the measured contrast is really a convolution of cell wall material TC and microstructure TC.

Unpublished Experimental Work

Introduction

Further experiments have been conducted on the topic of quantitative TC measurements by SThM, trying to obtain true quantitative values. A first approach was to try to replicate the work of Gomès et al. [46] on wood thin sections and evaporated thin layers as calibration standards. This approach failed due to imperfect contact to the support layer and non-smooth surface of the wood thin sections, however. Therefore, the approach was altered and instead embedded fibres were investigated. This resolves the problem of unknown sub-surface properties by basically providing a semi-infinite space for conduction. While examining the transversal TC was quickly discarded for the moment, analysis of the longitudinal TC shows some promise.

As results of those experiments were not yet at a publishable status at the time this thesis was written due to grave gaps in measurement technique and understanding, the experiment set-up and results so far as well as an outlook and suggestions on further development of the method are outlined below.

Table 1: Nominal thermal conductivities and diameters of tested fibres

	PP	G	K	C	Lyocell	P
λ $[Wm^{-1}K^{-1}]$	0.25	1.00	3.8	180	?	?
diameter [µm]	32	13	12	6.5	10	>10

Materials and Methods

The fibres used for calibration were polypropylene (PP), glass (G), aramide (A) and carbon (C). Regenerate cellulose (Lyocell, L), and beech wood pulp (P) were the test samples. All fibres are summarized in Table 1. The TC values of glass and carbon fibres were taken from the data sheet provided by the manufacturer. For PP, a value on the high end of the range suggested by various technical tables was taken. For A, the value given in the work by Ventura and Martelli [48] for room temperature was used. The carbon fibre was only used in the first two series, as it proved too hard and brittle to provide enough smooth sections for deriving useful TC values.

The fibres were embedded in epoxy, with the embedding procedure following the steps described by Konnerth et al. [39]. The epoxy provides dimensional stability for the fibres as well as a background of constant TC for the thermal measurements. Special care was taken that the orientation of the fibres in the finished sample was perpendicular to the planed surface. Since slight deviations for several fibres usually could not be prevented, only such with ideal orientation were selected by using out-of-focus optical microscopy. For pulp, the procedure deviated slightly in such way that small amounts of pulp were simply mixed with the epoxy. From the resulting random distribution of fibres and particles, suitable fibres were again picked by out-of-focus optical microscopy.

The SThM-tests were performed on a Bruker Dimension Icon AFM equipped for

SThM, with the standard Bruker SThM-tip in contact mode and a constant heating voltage of 1.5V. The bridge voltage was zeroed out before the start of the first test of a series with the tip heated and in contact, then kept unchanged for the whole test series. To prevent possible influence of varying heating gradients or overheating of the tip, heat voltage was only applied 10 seconds before the tip-sample approach, and was turned off when the tip was lifted off the sample. Scan size for tests varied from 20µm to 40µm for different test series, with a scanning speed between .7Hz and 0.3Hz, respectively. The feedback and setpoint parameters were set during the first scan of a test series and subsequently kept constant at high feedback and lowest possible force for the entire series (slight adjustments to feedback parameters when necessary). Each series consisted of 2-3 images for each fibre type + 1 image of the pure epoxy background for this sample.

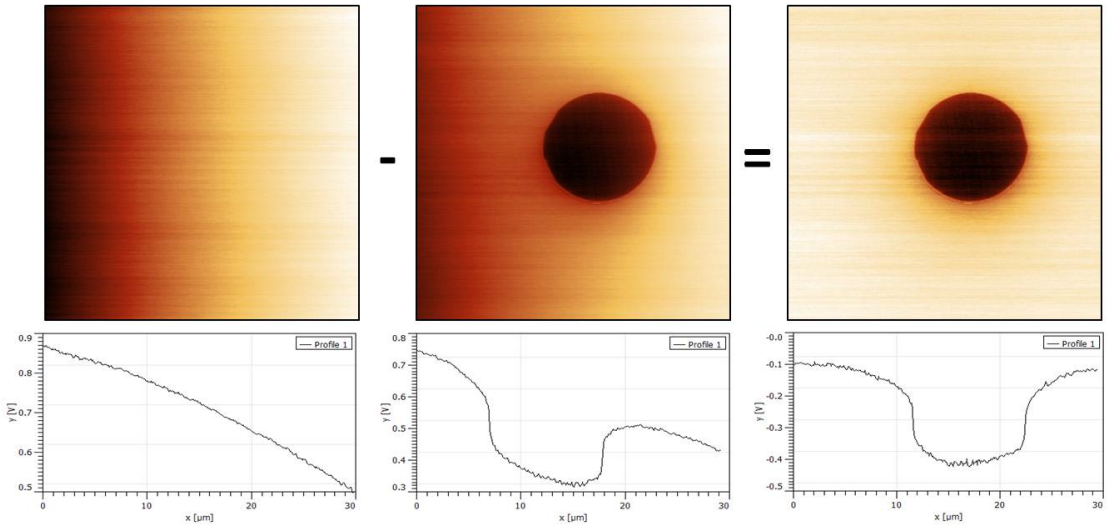

Figure 5: Image correction for CC images to filter tilt

AFM image processing and analysis was performed using the free software Gwyddion (V. 2.33). The topography images were corrected for plane-shift of the epoxy surface (<1°) and the z-value shifted such that the mean z-value of the epoxy background was zero to allow better comparison. All conductivity contrast (CC) images were corrected

for a constant background tilt which was independent of topography tilt by scanning the pure epoxy background of the respective sample and subtracting it from the fibre images of that sample (Figure 5). The CC was analysed as the difference between the epoxy background and the fibre for each image. When applying the mask for evaluation, care was taken to always keep the same pixel distance towards the fibre edge for each image, as those showed (especially for the epoxy $\rightarrow$ fibre transition) considerable gradients.

Results and Discussion

Figure 6 shows some light micrographs taken with the AFM-internal microscope (a), as well as topography (b) and CC (c) images for all sample types. All AFM images have the same z-resolution (height and CC, respectively) to allow comparison. The topography image shows little to no steps between fibre and epoxy in general. However, the glass fibre shows signs of chipping, resulting in dents. The carbon fibre has large parts missing completely, resulting in deep holes, the effects of which can also be seen on the thermal channel, and microroughness on the rest of the surface, resulting in imperfect tip-sample contact. In result, the carbon fibre was ditched after the first series as no meaningful results could be obtained. The thermal image series shows an increasing CC in the order of PP<G<A, with L approximately the colour of G, P showing a bit higher contrast. The thermal channel images were then analysed for the fibre-epoxy contrast. The results for all test series are depicted in Figure 7. Applying a logarithmic fit to the calibration results allows to obtain values for the TC values of L and P (always depicted in the same colour as the series) from the equation of the fit. The logarithm is chosen as it best resembles the non-linear behaviour also described by Gomes et al. [46, 49] as well as make sense from a physical point of view

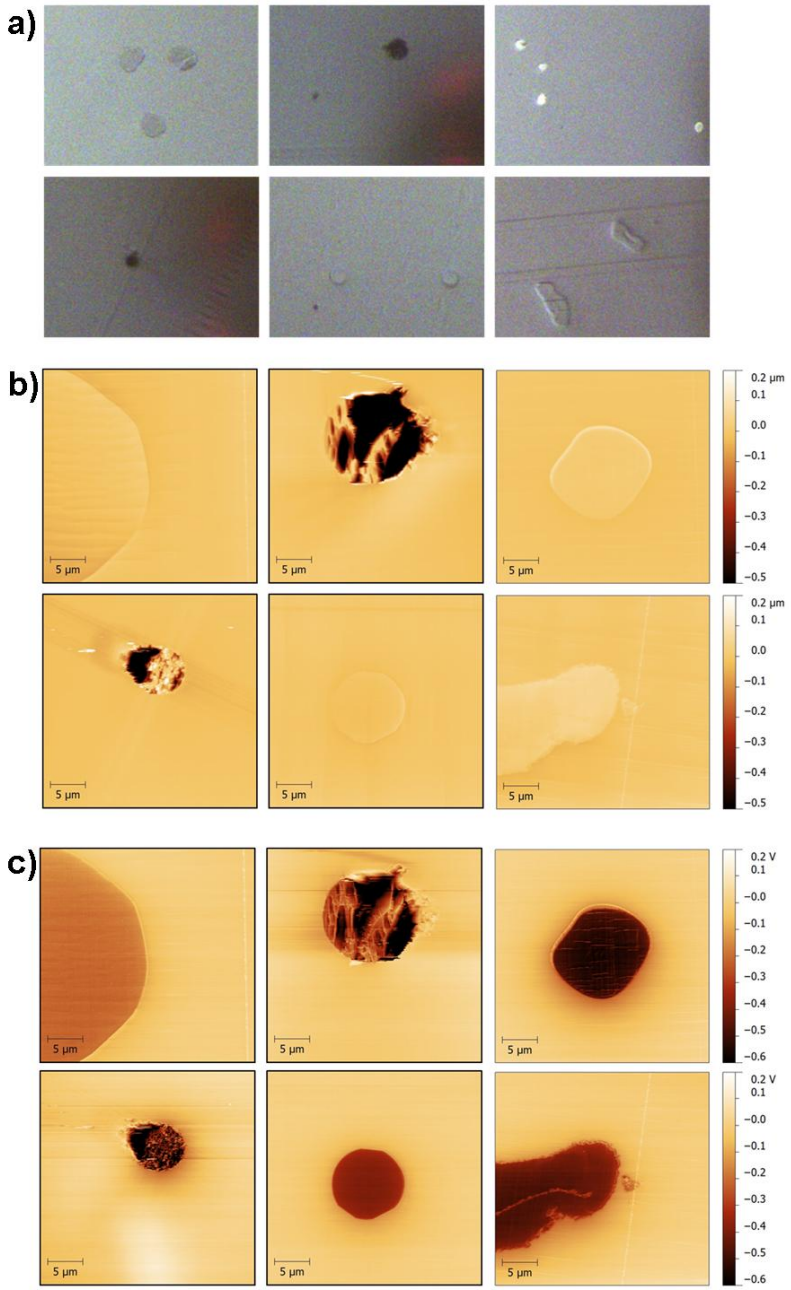

Figure 6: Light micrographs from AFM-internal microscope (a), AFM topography (b) and CC images (c) for all samples. The image order is PP - G - A above, C - L - P below. The topography shows high roughness/damage to glass and carbon fibres. However, the glass fibre shows some small, smooth areas which were evaluated. The CC shows the G and L fibres having approximately the same values, with PP well below and A higher. P seems a bit higher than L, but less than A. While C shows a high contrast, it is basically unusable due to the high damage and resulting roughness.

by allowing negative values for the CC (normalized on the epoxy) while approaching TC = $0 W m^{-1} K^{-1}$ asymptotically. As can be seen, the general results are quite reproducible, with similar values for L ($\sim$0.7$W m^{-1} K^{-1}$, 5 test series) and P ($\sim$0.95-1.1$W m^{-1} K^{-1}$, 2 test series).

However, with only three calibration samples only the minimum amount for a non-linear fit is provided. Also, in most cases, the G value is well below the fit curve, with about the same CC values as L, but an assumed TC of $1 W m^{-1} K^{-1}$. It is assumed that this mostly result from the rough surface, though, as the one series where it actually is on the curve was the only one where most of the glass fibre was smooth.

The main problem is therefore the limited amount of samples with the right properties: melting point > 100°C, fibrous, TC = 0.2 < $5 W m^{-1} K^{-1}$, non-brittle and homogeneous. Those properties mostly apply to polymers. These, however, usually have TC values ranging from 0.1 to $0.5 W m^{-1} K^{-1}$, which is well below the range where an exact calibration is needed for cellulose materials ($\sim 1 W m^{-1} K^{-1}$) as suggested by Eitelberger and Hofstetter[37]. Another problem with polymer fibres is their anisotropy due to the production process, resulting in a factor of doubt as to the true TC in fibre direction. Another less apparent problem of the results so far is the 0-contrast value, e.g. the value of the epoxy. According to the fits, the corresponding TC values would be around 0.04 - $0.05 W m^{-1} K^{-1}$, a value close to the TC of ambient air. Gomes et al [50] have shown that in SThM the major amount of heat (75-90%) is dissipated via ambient air. This might explain this value to some extend, suggesting that at any moment, what is measured is basically ambient air, and only by taking the different behaviour to the epoxy background the different values arise. However, it seems at least strange that all fibres, even the PP with a TC of $0.2 W m^{-1} K^{-1}$, show a higher TC in comparison to the epoxy, which can take a wide range of conductivities but usually should be around $0.5 W m^{-1} K^{-1}$. Unfortunately, even the epoxy manufacturer

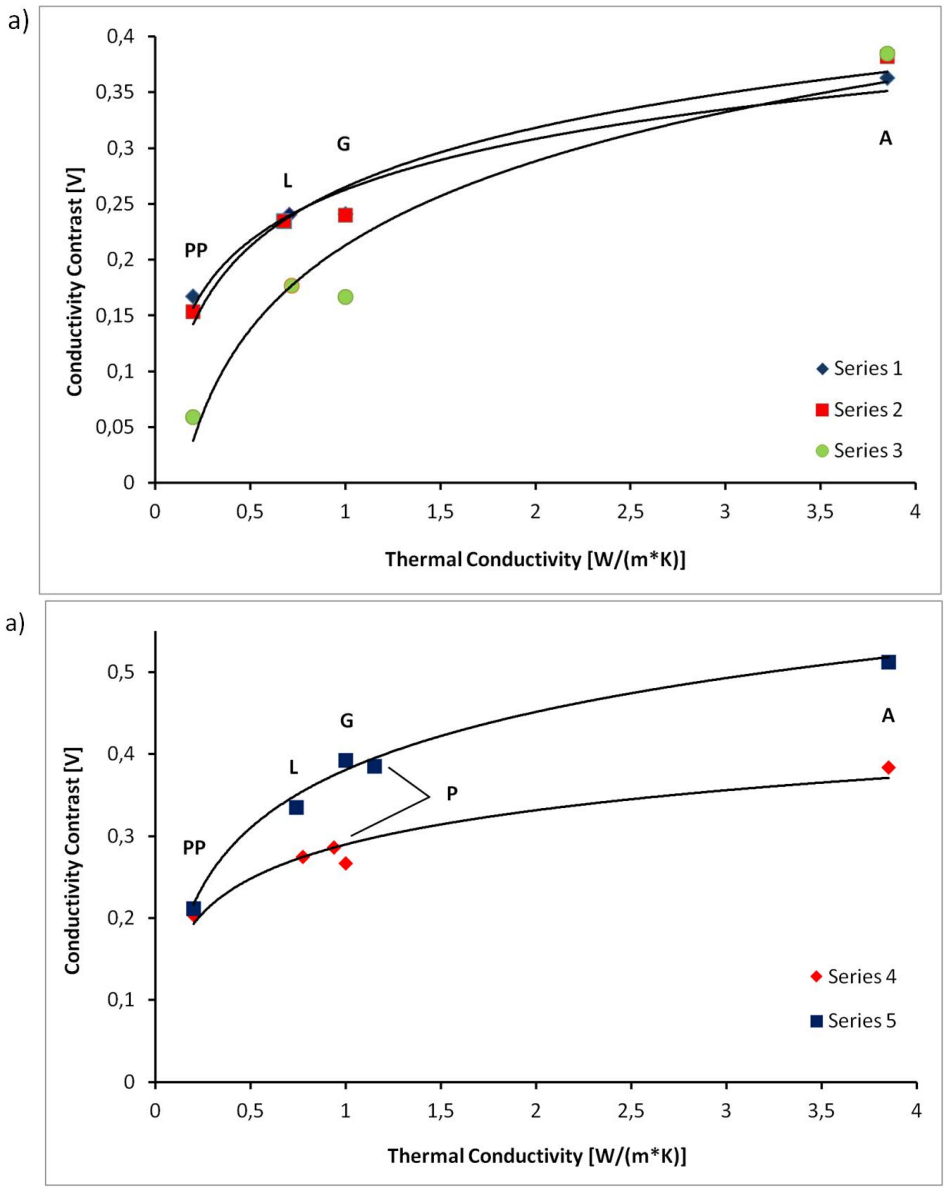

Figure 7: CC vs. TC for series 1-3 (a; only L as test sample) and series 4-5 (b; L and P as test samples). The values for L (~$0.7 W m^{-1} K^{-1}$) and P (~$1 W m^{-1} K^{-1}$) are mostly constant and reasonable. With the exception of Series 5, G always takes a too small contrast values, probably due to the non-smooth surface. The large variation between curves shows the necessity of series-inherent calibration.

was not able to provide more detailed information on the thermal properties of the epoxy in use.

One thing the high dissipation via ambient air could explain however, is why the fibre diameter does not seem to pose a problem for the tests, since the by far largest amount of heat is dissipated from the cantilever via air towards the epoxy, which takes >99% of the total sample surface. Another problem that needs to be addressed is the continuity in measurements. During this series of tests, each time the system was allowed to fully cool down and then reheated (basically over night), the values became non-compatible with those previously obtained, reducing the maximum time for one series to a day of non-interrupted tests, giving a maximum of 1-2 test samples that could be tested with three images per sample.

Still, even with these problems, the author strongly believes in the general feasibility and potential usefulness of this technique. To this ends, a two-way approach is suggested. First off, the creation of a proper set of calibration samples. For natural fibre analysis, this should consist of at least 5 or more samples with TC values in the range of 0.4$Wm^{-1}K^{-1}$ (lignin, [37]) to 1$Wm^{-1}K^{-1}$ (cellulose chain-parallel, [37]), with aramide providing a high end. While one or two materials with high conductivities could be helpful for a fit curve, the TC resolution of SThM becomes rather low at values >20$Wm^{-1}K^{-1}$ [49, 50, 51]. All fibres would need to be well characterized for their specific TC and anisotropy, as those parameters can vary widely for polymers and tabulated data seems not too dependable (with suggested values often varying by a factor of 2). Ideally all fibres should have an approximately equal diameter, though as pointed out this seems not strictly necessary. Also, fibres with an easy to regenerate surface (by planing with microtome or polishing) should be preferred. The epoxy background should also be well characterized at this point.

The other problem that needs to be tackled is the theoretical understanding of the

heat transportation and conduction process. For an amorphous surface, such work already exists [51]. However, the specific problem of a semi-infinite sample consisting of a fibre embedded in a matrix should be specifically researched. A good method to do so might be a numerical computational approach, as this would allow for more parameters to be taken into account than a purely analytical approach. A main point that needs explanation is the shape of the CC-TC-curve and the differences in conduction behaviour between the (supposedly) isotropic matrix and the anisotropic fibres.

With solutions to those problems, this method could provide a simple and straightforward method for obtaining quantitative values for the TC of fibrous materials, with the available methods needing more work and preparation (e.g. [52]) or are only applicable for high conductivities [53].

Conclusion

The aim of this thesis was to introduce, develop and apply analysis methods on and below the micrometer scale in the field of natural fibre research. CS-NI was developed as a means to obtain high resolution adhesion data, as demonstrated on a model system (Paper 1). An application of this method was demonstrated in Paper 2, where the different adhesive behaviour of the S2 and S3 cell wall layer were shown for 2 common adhesive types. These works demonstrate the principle applicability and utility of this method. The ability to single out the parameter of cell wall-adhesive interaction could provide valuable new insights in the important topic of wood adhesion, comparable to e.g the single-fibre pull-out test in the field of fibre composites research. While the method is readily applicable, a focus for future development should be an improved understanding of the deformation processes involved. A working model, theoretical or computational, able to extract the specific energy of adhesion from the total indentation energy and material parameters of cell wall and adhesive, would allow to compare different adhesives with this method.

The analysis of the effect of nanoscale roughness on the optical appearance of natural fibres was analysed in Paper 3. While a clear influence was demonstrated, no quantification could be given at this point due to parallel changes in surface chemistry. Further experiments in planning intent to investigate the possibility of controlling optical appearance by controlling the parameter of nanoroughness. For Paper 4, position

and time dependent changes in surface polarity of the wood cell wall were measured by the rather novel QNM method. It shows that especially the fresh-cut S2 layer shows a strong decrease in polarity. In combination with the results presented in Paper 2, this work could provide an impact on wood technology in aspect of norms and standards for bonding wood. In Paper 5, SThM was shown as method to analyse TC directly at the wood cell wall. While the method is still very rudimentary in aspect of extracting quantitative results, it is strongly believed that it could prove a strong and versatile tool in the whole field of natural fibre science, could the problems outlined in the experimental section be overcome.

List of Figures

Bibliography

[1] "Annual world production." [Online]. Available: http://inventor.grantadesign.com/en/notes/science/material/C04 Annual world production.htm

[2] P. Niemz, *Holz, in 3 Bdn., Physik des Holzes und der Holzwerkstoffe*, auflage: 1 ed. Leinfelden-Echterdingen: DRW-Verlag.

[3] F. P. L. U. F. Service, "Wood handbook: Wood as an engineering material," vol. 190.

[4] W. Oliver and G. Pharr, "Improved technique for determining hardness and elastic modulus using load and displacement sensing indentation experiments," *Journal of Materials Research*, vol. 7, no. 6, pp. 1564–1580, 1992.

[5] ——, "Measurement of hardness and elastic modulus by instrumented indentation: Advances in understanding and refinements to methodology," *Journal of Materials Research*, vol. 19, no. 1, pp. 3–20, 2004.

[6] R. Wimmer, B. Lucas, T. Tsui, and W. Oliver, "Longitudinal hardness and young's modulus of spruce tracheid secondary walls using nanoindentation technique," *Wood Science and Technology*, vol. 31, no. 2, pp. 131–141, 1997.

[7] L. Bertinetti, U. Hangen, M. Eder, P. Leibner, P. Fratzl, and I. Zlotnikov, "Characterizing moisture-dependent mechanical properties of organic materials: humidity-controlled static and dynamic nanoindentation of wood cell walls," 2014.

[8] T. Bader, K. de Borst, K. Fackler, T. Ters, and S. Braovac, "A nano to macroscale study on structure-mechanics relationships of archaeological oak," *Journal of Cultural Heritage*, vol. 14, no. 5, pp. 377–388, 2013.

[9] F. Stoeckel, J. Konnerth, and W. Gindl-Altmutter, "Mechanical properties of adhesives for bonding wood-a review," *International Journal of Adhesion and Adhesives*, vol. 45, pp. 32–41, 2013.

[10] J. Beaugrand, M. Nottez, J. Konnerth, and A. Bourmaud, "Multi-scale analysis of the structure and mechanical performance of woody hemp core and the dependence on the sampling location," *Industrial Crops and Products*, vol. 60, pp. 193–204, 2014.

[11] L. Wagner, T. Bader, and K. De Borst, "Nanoindentation of wood cell walls: Effects of sample preparation and indentation protocol," *Journal of Materials Science*, vol. 49, no. 1, pp. 94–102, 2014.

[12] J. Jakes, C. Frihart, J. Beecher, R. Moon, P. Resto, Z. Melgarejo, O. Suárez, H. Baumgart, A. Elmustafa, and D. Stone, "Nanoindentation near the edge," *Journal of Materials Research*, vol. 24, no. 3, pp. 1016–1031, 2009.

[13] J. Jakes, C. Frihart, J. Beecher, R. Moon, and D. Stone, "Experimental method to account for structural compliance in nanoindentation measurements," *Journal of Materials Research*, vol. 23, no. 4, pp. 1113–1127, 2008.

[14] J. Sánchez, S. El-Mansy, B. Sun, T. Scherban, N. Fang, D. Pantuso, W. Ford, M. Elizalde, J. Martínez-Esnaola, A. Martín-Meizoso, J. Gil-Sevillano,

M. Fuentes, and J. Maiz, "Cross-sectional nanoindentation: A new technique for thin film interfacial adhesion characterization," *Acta Materialia*, vol. 47, no. 17, pp. 4405–4413, 1999.

[15] M. Elizalde, J. Sánchez, J. Martínez-Esnaola, D. Pantuso, T. Scherban, B. Sun, and G. Xu, "Interfacial fracture induced by cross-sectional nanoindentation in metal-ceramic thin film structures," *Acta Materialia*, vol. 51, no. 14, pp. 4295–4305, 2003.

[16] G. Binnig, C. F. Quate, and C. Gerber, "Atomic force microscope," *Phys. Rev. Lett.*, vol. 56, no. 9, pp. 930–933, Mar. 1986.

[17] T. Pesacreta, L. Groom, and T. Rials, "Atomic force microscopy of the intervessel pit membrane in the stem of sapium sebiferum (euphorbiaceae)," *IAWA Journal*, vol. 26, no. 4, pp. 397–426, 2005.

[18] A. Olszewska, P. Eronen, L.-S. Johansson, J.-M. Malho, M. Ankerfors, T. Lindström, J. Ruokolainen, J. Laine, and M. Österberg, "The behaviour of cationic NanoFibrillar cellulose in aqueous media," *Cellulose*, vol. 18, no. 5, pp. 1213–1226, 2011.

[19] R. Lahiji, X. Xu, R. Reifenberger, A. Raman, A. Rudie, and R. Moon, "Atomic force microscopy characterization of cellulose nanocrystals," *Langmuir*, vol. 26, no. 6, pp. 4480–4488, 2010.

[20] T. Pesacreta, L. Carlson, and B. Triplett, "Atomic force microscopy of cotton fiber cell wall surfaces in air and water: Quantitative and qualitative aspects," *Planta*, vol. 202, no. 4, pp. 435–442, 1997.

[21] M. Meincken and P. Evans, "Nanoscale characterization of wood photodegradation using atomic force microscopy," *European Journal of Wood and Wood Products*, vol. 67, no. 2, pp. 229–231, 2009.

[22] J. Fahlén and L. Salmén, "Pore and matrix distribution in the fiber wall revealed by atomic force microscopy and image analysis," *Biomacromolecules*, vol. 6, no. 1, pp. 433–438, 2005.

[23] A. Baker, W. Helbert, J. Sugiyama, and M. Miles, "Surface structure of native cellulose microcrystals by AFM," *Applied Physics A: Materials Science and Processing*, vol. 66, no. SUPPL. 1, pp. S559–S563, 1998.

[24] R. De la Rie, "The influence of varnishes on the appearance of paintings," *Studies in conservation*, vol. 32, pp. 1–13, 1987.

[25] S. Watanabe, H. Sato, S. Shibuichi, M. Okamoto, S. Inoue, and N. Satoh, "Formation of nanostructure on hair surface: Its characteristic optical properties and application to hair care products," *Journal of Cosmetic Science*, vol. 58, no. 4, pp. 283–294, 2007.

[26] A. Noy, D. Vezenov, and C. Lieber, "Chemical force microscopy," *Annual Review of Materials Science*, vol. 27, no. 1, pp. 381–421, 1997.

[27] H.-J. Butt, B. Cappella, and M. Kappl, "Force measurements with the atomic force microscope: Technique, interpretation and applications," *Surface Science Reports*, vol. 59, no. 1–6, pp. 1–152, Oct. 2005.

[28] J. Bastidas, R. Venditti, J. Pawlak, R. Gilbert, S. Zauscher, and J. Kadla, "Chemical force microscopy of cellulosic fibers," *Carbohydrate Polymers*, vol. 62, no. 4, pp. 369–378, 2005.

[29] A. Pietak, S. Korte, E. Tan, A. Downard, and M. Staiger, "Atomic force microscopy characterization of the surface wettability of natural fibres," *Applied Surface Science*, vol. 253, no. 7, pp. 3627–3635, 2007.

[30] A. Klash, E. Ncube, and M. Meincken, "Localization and attempted quantification of various functional groups on pulpwood fibres," *Applied Surface Science*, vol. 255, no. 12, pp. 6318–6324, 2009.

[31] R. Lahiji, Y. Boluk, and M. McDermott, "Adhesive surface interactions of cellulose nanocrystals from different sources," *Journal of Materials Science*, vol. 47, no. 9, pp. 3961–3970, 2012.

[32] F. Kollmann and L. Malmquist, "Über die wärmeleitzahl von holz und holzwerkstoffen," *Holz als Roh-und Werkstoff*, vol. 14, no. 6, pp. 201–204, Jun. 1956.

[33] B. Suleiman, J. Larfeldt, B. Leckner, and M. Gustavssor, "Thermal conductivity and diffusivity of wood," *Wood Science and Technology*, vol. 33, no. 6, pp. 465–473, 1999.

[34] "Datenbank." [Online]. Available: http://www.ifb.ethz.ch/wood/database

[35] J. Hunt and H. Gu, "Two-dimensional finite element heat transfer model of softwood. part i. effective thermal conductivity," *Wood and Fiber Science*, vol. 38, no. 4, pp. 592–598, 2006.

[36] H. Thoemen, T. Walther, and A. Wiegmann, "3d simulation of macroscopic heat and mass transfer properties from the microstructure of wood fibre networks," *Composites Science and Technology*, vol. 68, no. 3-4, pp. 608–616, 2008.

[37] J. Eitelberger and K. Hofstetter, "Prediction of transport properties of wood below the fiber saturation point - a multiscale homogenization approach and its experimental validation. part i: Thermal conductivity," *Composites Science and Technology*, vol. 71, no. 2, pp. 134–144, 2011.

[38] J. Konnerth, N. Gierlinger, J. Keckes, and W. Gindl, "Actual versus apparent within cell wall variability of nanoindentation results from wood cell walls related to cellulose microfibril angle," *Journal of Materials Science*, vol. 44, no. 16, pp. 4399–4406, 2009.

[39] J. Konnerth, D. Harper, S.-H. Lee, T. Rials, and W. Gindl, "Adhesive penetration of wood cell walls investigated by scanning thermal microscopy (SThM)," *Holzforschung*, vol. 62, no. 1, pp. 91–98, 2008.

[40] C. Gibson, D. Smith, and C. Roberts, "Calibration of silicon atomic force microscope cantilevers," *Nanotechnology*, vol. 16, no. 2, pp. 234–238, 2005.

[41] B. Ohler, "Cantilever spring constant calibration using laser doppler vibrometry," *Review of Scientific Instruments*, vol. 78, no. 6, 2007.

[42] K. Ramirez-Aguilar and K. Rowlen, "Tip characterization from AFM images of nanometric spherical particles," *Langmuir*, vol. 14, no. 9, pp. 2562–2566, 1998.

[43] D. Tranchida, S. Piccarolo, and R. Deblieck, "Some experimental issues of AFM tip blind estimation: The effect of noise and resolution," *Measurement Science and Technology*, vol. 17, no. 10, pp. 2630–2636, 2006.

[44] G. Fiege, A. Altes, R. Heiderhoff, and L. Balk, "Quantitative thermal conductivity measurements with nanometre resolution," *Journal of Physics D: Applied Physics*, vol. 32, no. 5, pp. L13–L17, 1999.

[45] S. Lefevre and S. Volz, "3ω-scanning thermal microscope," *Review of Scientific Instruments*, vol. 76, no. 3, 2005.

[46] S. Gomès, L. David, V. Lysenko, A. Descamps, T. Nychyporuk, and M. Raynaud, "Application of scanning thermal microscopy for thermal conductivity measurements on meso-porous silicon thin films," *J. Phys. D: Appl. Phys.*, vol. 40, no. 21, p. 6677, Nov. 2007. [Online]. Available: http://iopscience.iop.org/0022-3727/40/21/029

[47] M. Scheikl and M. Dunky, "Measurement of dynamic and staue contact angles on wood for the determination of its surface tension and the penetration of liquids into the wood surface," *hfsg*, vol. 52, no. 1, pp. 89–94, 2009. [Online]. Available: http://www.degruyter.com/view/j/hfsg.1998.52.issue-1/hfsg.1998.52.1.89/hfsg.1998.52.1.89.xml

[48] G. Ventura and V. Martelli, "Thermal conductivity of kevlar 49 between 7 and 290 k," *Cryogenics*, vol. 49, no. 12, pp. 735–737, 2009.

[49] S. Gomès, P. Newby, B. Canut, K. Termentzidis, O. Marty, L. Fréchette, P. Chantrenne, V. Aimez, J.-M. Bluet, and V. Lysenko, "Characterization of the thermal conductivity of insulating thin films by scanning thermal microscopy," *Microelectronics Journal*, vol. 44, no. 11, pp. 1029–1034, 2013.

[50] S. Gomes, N. Trannoy, P. Grossel, F. Depasse, C. Bainier, and D. Charraut, "D.c. scanning thermal microscopy: Characterisation and interpretation of the measurement," *International Journal of Thermal Sciences*, vol. 40, no. 11, pp. 949–958, 2001.

[51] L. David, S. Gomès, and M. Raynaud, "Modelling for the thermal characterization of solid materials by dc scanning thermal microscopy," *Journal of Physics D: Applied Physics*, vol. 40, no. 14, pp. 4337–4346, 2007.

[52] T. Yamane, S.-I. Katayama, M. Todoki, and I. Hatta, "Thermal diffusivity measurement of single fibers by an ac calorimetric method," *Journal of Applied Physics*, vol. 80, no. 8, pp. 4358–4365, 1996.

[53] J. Wang, M. Gu, X. Zhang, and Y. Song, "Thermal conductivity measurement of an individual fibre using a t type probe method," *Journal of Physics D: Applied Physics*, vol. 42, no. 10, 2009.

APPENDIX

Paper 1 - Determination of Adhesive Energy at the Wood Cell-Wall/UF Interface by Nanoindentation (NI)

Holzforschung, Vol. 66, pp. 781–787, 2012 • Copyright © by Walter de Gruyter • Berlin • Boston. DOI 10.1515/hf-2011-0205

Determination of adhesive energy at the wood cell-wall/UF interface by nanoindentation (NI)

Michael Obersriebnig, Stefan Veigel, Wolfgang Gindl-Altmutter* and Johannes Konnerth

Department of Materials Science and Process Technology, BOKU – University of Natural Resources and Life Science, Vienna, Austria

*Corresponding author.
Department of Materials Science and Process Technology, BOKU – University of Natural Resources and Life Science Vienna, Konrad Lorenz Strasse 24, A-3430 Tullin, Austria
Phone: +43-1-47654-4255
Fax: +43-1-47654-4295
E-mail: wolfgang.gindl-altmutter@boku.ac.at

Abstract

Spruce wood specimens were surface-silylated according to three different protocols in order to progressively reduce hydrophilicity and, consequently, adhesion to urea-formaldehyde (UF) glue. Compared to the untreated reference, the macroscopic adhesive strength was drastically reduced in silylated specimens. Specimens treated with the most effective silylation method in terms of reduction of hydrophilicity showed near zero adhesion to UF glue. Micromechanical characterisation by means of nanoindentation (NI, Berkovich-type probe) revealed that the wood cell wall stiffness and hardness was not significantly affected by silylation. Contrarily, NI experiments (conical indenter tip with 60° opening angle) performed directly at the interface between the wood cell wall and the adhesive showed significantly reduced hardness and reduced specific work of NI in silylated specimens. It is concluded that the measured correlation between reduced hydrophilicity in silylated specimens and the mechanical strength of the interface is due to reduced adhesion. This allows calculating the specific adhesive energy for the system wood cell wall-urea formaldehyde glue from the difference between the specific work of adhesion obtained from the unmodified reference and the most efficiently silylated specimen. The advantage of this new method lies in the position-resolved measurement of qualitative differences in adhesive energy directly at the interface. This is not feasible with macroscopic test methods, which also include effects of surface roughness, cellular adhesive penetration, or grain angle.

Keywords: adhesive bond line; adhesive energy; nanoindentation (NI); urea-formaldehyde (UF); wood glueing.

Introduction

The quantification of adhesion between solid phases in a composite material, be it of biological or man-made origin, is essential for a more comprehensive understanding of its properties. At the macroscopic scale, different types of shear-, delamination-, or fracture tests may be employed (e.g., Konnerth et al. 2006; Singh et al. 2010; Clauss et al. 2011; Sahaf et al. 2012), whereas a direct characterisation of adhesion at the microscopic scale is more challenging. The strength of adhesive bonds between reinforcement fibre and matrix in fibre-reinforced composites can be determined by means of micro-bond testing on model single-fibre composites (Gaur and Miller 1989; Drzal et al. 2000; Zhandarov and Mäder 2005).

Atomic force microscopy (AFM) and nanoindentation (NI) techniques provide some insight into the variability of certain mechanical characteristics at the transition between fibre and matrix (Gao and Mäder 2002; Lee et al. 2009). While the microstructure of fibre-reinforced composites or, even more so, single-fibre model composites, is fairly simple, great complexity is found at the same scale in wood-based composite materials like medium density fibreboard (MDF) or particleboard. As wood has to be disintegrated to varying degrees in the processing of wood-based composites, one has to deal with particles of different size, geometry and surface roughness.

Also the chemical characteristics of wood surfaces and wood fibres may vary depending on species and treatment (de Meijer et al. 2000; Gindl and Tschegg 2002; Peterlin et al. 2010). Thus a method is needed, which is independent of the influence of these additional parameters. Once adhesion can be characterised directly at the cellular scale, effects of varying surface chemistry can be studied in combination with various adhesives and related to different wood species or pre-treated wood.

In this context, NI experiments performed directly at the interface between the cell wall and the cured adhesive is a good candidate for problem solution. The NI approach was useful for the characterisation of ceramic-ceramic adhesion (Sánchez et al. 1999). The adhesion of Si_xN_y/SiO films to a Si-substrate was measured by performing indents into the substrate on the cross section of the sample. For NIs, a Berkovich-type probe was used, with the near side of the triangular pyramid parallel to the interface.

Because of the brittleness of the substrate, a crack propagates and eventually reaches and follows the line of adhesion, leading to delamination. By measuring the delaminated area and the NI work, a measure for the strength of adhesion

is obtained. As means of verification, the critical interfacial energy release rate G_{ci} was compared to model calculations based on the plate model of elasticity, yielding good agreement between the results. The technique was adapted to thin film metal-ceramic interfaces (Elizalde et al. 2003) and patterned structures (Molina-Aldareguia et al. 2007; Roy et al. 2007).

All approaches described above are limited to brittle substrates and can therefore not be directly applied to a relatively ductile wood cell wall-adhesive system, where crack generation can hardly be expected. Therefore, surface-modified specimens having very low-adhesion propensity were chosen for the present study as reference. The underlying assumption is the following: when a sharp indenter tip is penetrated exactly at the interface between the wood cell wall and the cured adhesive, the energy spent to achieve a certain depth of NI will be the sum of the work required for plastic and elastic deformation of adhesive and adherend, and the work required for separation of the adhesive from the adherend.

When a specimen with an adhesion close to zero is available, the total work of NI should be smaller than the work spent in case of a specimen with strong adhesion. Assuming that the work required for plastic and elastic deformation of adhesive and adherend is the same in both sets of specimens, a final difference in the total NI work will roughly correspond to the work of adhesion. The present study investigates the principal feasibility of such a NI-based method for the measurement of adhesion in wood-based composites at cellular scale.

Materials and methods

Surface modification

Norway spruce wood specimens with a length of 50 mm and a cross section of 10 mm×5 mm were subjected to three different silylation treatments. 1) Silylation with dichlorodiphenylsilane (DPS) following exactly the procedure of Mohammed-Ziegler et al. (2006). Briefly, the specimens were treated for 1 h under continuous stirring in a 1% (v/v) n-hexane solution of DPS. Then the samples were rinsed with n-hexane and air-dried. 2) A set of specimens was subjected to a two-step treatment with octadecyltrichlorosilane (OTS) and chlorotrimethylsilane (CTMS) (Mohammed-Ziegler et al. 2006). The procedure consists of a 1st silylation step, in which the specimens are treated in a 1% (v/v) n-hexane solution of OTS for 1 h under continuous stirring with

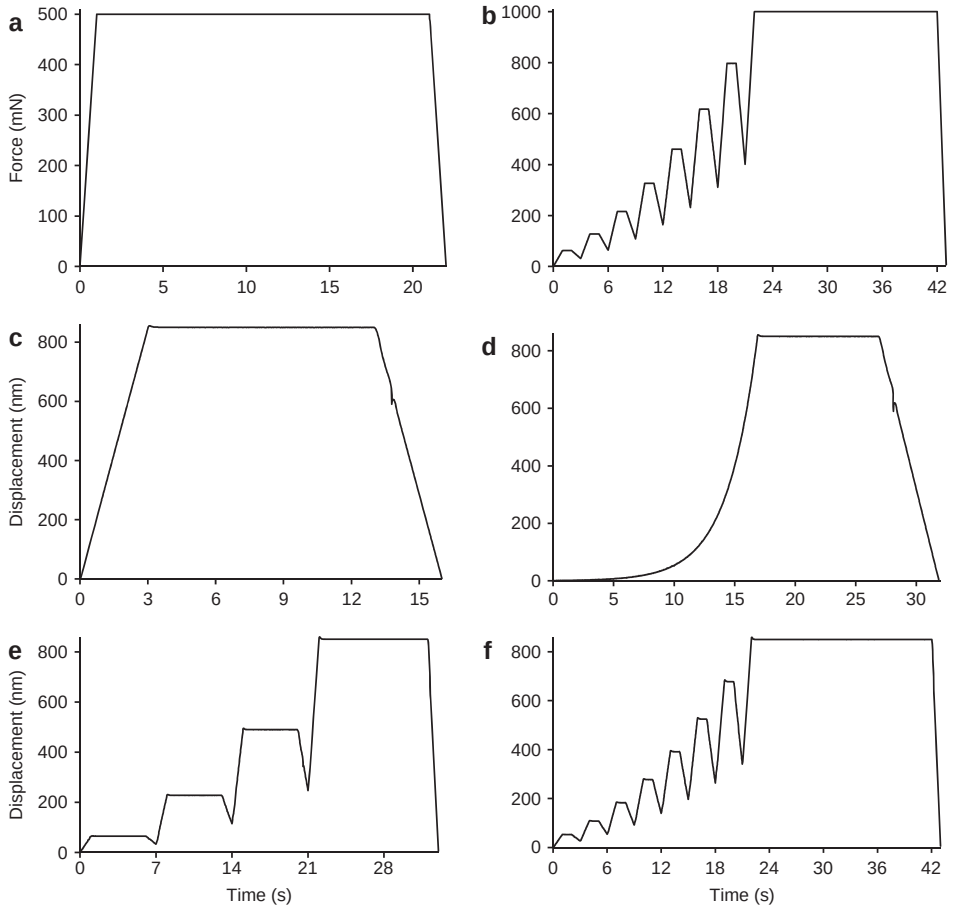

Figure 1 Load functions utilised during NI experiments. (a) Material characterisation; (b) adhesion test, force controlled; peak load increases with t squared; (c–f) adhesion test, displacement controlled load functions (LF1–4); for (d–f), peak displacement increases exponentially (d) or with t squared (e–f), respectively.

subsequent rinsing with n-hexane. After three days of air drying, the second silylation step is performed with a 1% (v/v) n-hexane solution of CTMS. The samples were rinsed with n-hexane and air-dried. 3) A set was modified with γ-aminopropyltriethoxysilane (APTES) (Hansmann et al. 2005). The samples were first immersed in cyclohexane for 20 min at approximately 60°C. Thereafter, APTES was added drop by drop up to a concentration of 1% (v/v), as well as small amounts of CTMS and pyridine. The reaction was carried out for 3 h under continuous stirring. The samples were rinsed with cyclohexane and dried at 103°C for 24 h.

The static contact angles

CA of deionised water on unmodified and modified wood surfaces were measured with the sessile drop method (Scheikl and Dunky 1998).

Adhesive bonding and macroscopic bond strength

Untreated reference specimens and the three groups of surface-modified specimens were bonded by means of UF adhesive (Prefere 10F152, Dynea, Austria). After several days of conditioning the bonded specimens were tested in tensile shear, whereby the overlap of the bonded pieces of wood was 10 mm. Specimens not tested served for further characterisation.

Nanoindentation (NI)

Small pieces of wood containing the adhesive bond line were prepared and embedded in epoxy resin by means of vacuum treatment. A smooth surface perpendicular to the direction of wood cells was then prepared by means of sectioning with a diamond knife mounted to an ultramicrotome. Instrument: Hysitron nanoindenter (Hysitron, Minneapolis, MN, USA). Wood cell walls and cured adhesive were indented with a Berkovich-type tip with a total opening angle of 142.3°, utilising a linear three-phase load function (Figure 1a).

For NI experiments directly into the interface between adhesive and wood cell wall, a cone-shaped tip with an opening angle of only 60° and a tip radius of 10 nm was applied. Such geometry leads to a larger force component transverse to the direction of loading in comparison to the flat Berkovich geometry. Accordingly, a more pointed indenter tip should therefore show a higher sensitivity to the strength of adhesion between the cell wall and the adhesive. A first experiment was performed in load control mode utilising an eight-step load function, where each step consisted of a 3 s load/hold/unload-phase, an increasing peak load for each step and a 20 s hold-phase for the last step (Figure 1b). The stepwise load function was intended to facilitate the detection of sudden changes, e.g., by

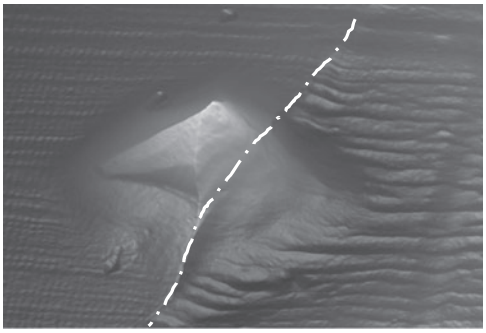

Figure 3 AFM image of a slightly misplaced residual indent at the cell wall (left) – adhesive (right) interface inverted for easier viewing. The crack path is outlined with a white line following the interface.

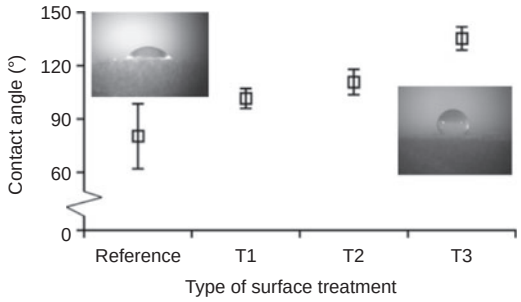

Figure 4 Increase of the contact angle between deionised water and the wood surface due to different surface treatments (T1: APTES, T2: DPS, and T3: OTS+CTMS).

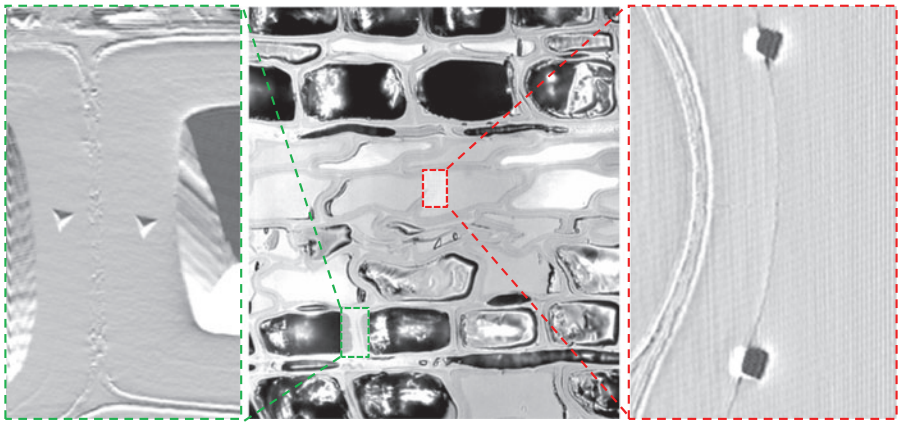

Figure 2 Microscope images showing the positioning of indents. Centre: incident light micrograph of an adhesive bondline with adhesive-filled wood cells. Left: SPM image of double cell walls with indents after characterisation by nanoindentation with a Berkovich tip. Right: SPM image of the interface between the cell wall and the adhesive characterised by nanoindentation with a 60° conical tip.

crack generation, in the specimen, which, however, did not occur. A second experiment was performed using various displacement controlled load functions with peak displacements of 850 nm as depicted in Figure 1c–f.

The locations for NI experiments were chosen in the incident light microscope (Figure 2) with precise positioning performed from scanning probe micrographs taken with the indenter tip. After each experiment, the accuracy of positioning was verified by means of another scan of the respective specimen area (Figure 2). Small deviations of the indent position around the bond line showed no observable influence on the results obtained. This is surprising at the first view. Explanation: the path of a crack takes in such a case a direction as revealed by AFM imaging of residual indents (Figure 3). Even when the indenter tip misses the interface by a few tens of nanometres, the stress field eventually reaches the interface at a certain NI depth and the crack path starts to follow the interface.

Data collected: hardness, NI depth, NI modulus (calculated according to Oliver and Pharr 1992), and the total work of NI (calculated by integrating the area under the load-depth curve).

Results and discussion

Macroscopic characterisation

All experiments showed strong effects of the chemical surface treatments on surface polarity and adhesive bonding. CA measurements with deionised water, as a simple method to determine hydrophobicity of surfaces, revealed significant changes (Figure 4). Assuming a direct relation between CA and the surface polarity, the untreated reference showed highest polarity, which decreased progressively after silylation treatment with APTES (T1)>DPS (T2)>OTS+CTMS (T3) (Figure 4). UF resin is a highly hydrophilic system (Scheikl and Dunky 1998). Therefore it is concluded that, similarly to water, the wettability with UF was decreased by the silylation treatments. This interpretation is supported by the results of the characterisation of macroscopic bond strength by shear testing (Figure 5). Compared to the untreated reference, a clear decrease is seen with increasing CA. With 0.2 MPa the specimens treated with OTS+CTMS retained only 2.7% of the bond strength of the reference.

Also, the failure mode changed from cohesive wood failure in the reference to pure adhesion failure at high CAs. Thus the

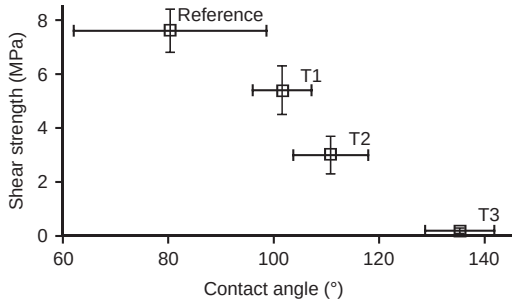

Figure 5 Macroscopic bond strength of differently treated wood-UF adhesive bonds related to wettability expressed by the contact angle with deionised water.

prerequisite for the envisaged NI experiments is given: on the one hand, a set of reference specimens with good adhesion is available, and on the other hand, a set of modified specimens with very little adhesion characteristic was obtained by surface silylation.

Nanoindentation (NI)

A first set of NI experiments performed with a Berkovich-type pyramid indenter tip was dedicated to the mechanical characterisation of cell wall and adhesive. As summarised in Figure 6, the cell wall modulus and hardness is not dependent significantly from the type of surface treatment. The magnitude of values measured is well within the range typically observed for wood cell walls (Gindl et al. 1998). In a similar manner, no clear dependencies are visible between the type of surface treatment and the mechanical characteristics of the cured UF resin (Figure 6).

Only the hardness values obtained for UF resin in an adhesive bond with OTS+CTMS treated specimens deviated significantly, showing an increase of 33%. In spite of this minor inconsistency, the overall result of the NI experiments is the following: 1) the silylation treatment did not significantly change the mechanical properties of wood cell walls, and 2) the silylation treatment did not inhibit the curing of the bulk UF. Hence a prerequisite for the next step in this study is fulfilled (unchanged mechanical properties of cell wall and

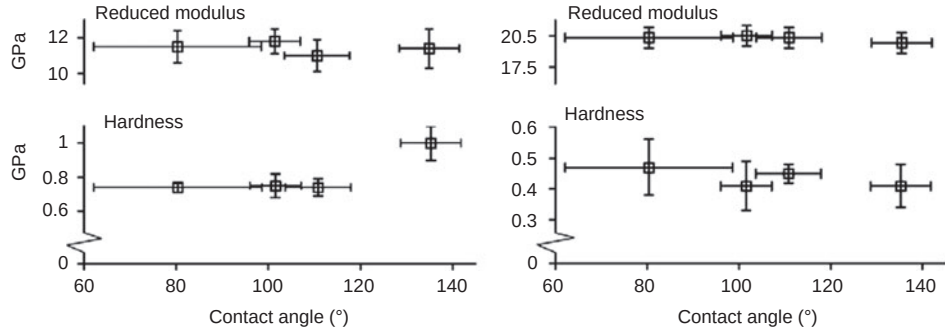

Figure 6 Results of the characterisation of cell walls and cured adhesive by means of nanoindentation in the untreated reference and in silylated specimens, which show different contact angles due to different treatments.

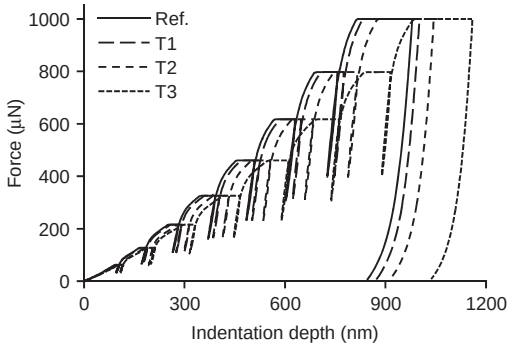

Figure 7 Mean force-displacement curves for four differently treated specimens obtained from performing indents at the cell wall-adhesive interface using an eight-step force controlled load function. The specimen with lowest macroscopic adhesive bond strength (T3) shows the biggest indentation depth at the chosen load.

adhesive). This shows that if differences in NI measurements will be observed, these can be interpreted as deviations in interface characteristics.

Two sets of experiments with different aims were performed directly at the cell wall-adhesive interface. The first experiment served to assess the principal feasibility of the chosen approach. All four groups of samples were tested under a force controlled load condition. The mean force-displacement curves are presented in Figure 7. The measured NI depth at peak load correlates well with the CA of water (Figure 4).

The difference in NI depth (Figure 7) is mainly attributable to deformation occurring during the hold phase, which could be interpreted as a varying degree of delamination at the interface depending on pre-treatment. In contrast, the slope of unload-load cycles, which depends on the elastic properties of the media, is almost identical for all treatments, and therefore the same NI modulus is measured for all samples. This first qualitative analysis is confirmed by numerical analysis of the NI modulus and hardness (Figure 8).

The NI modulus, which depends on the properties of the bulk adhesive and cell wall, shows no correlation with surface treatment. This goes well in line with results presented

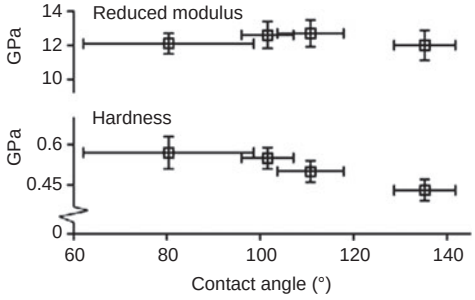

Figure 8 Results of indentation experiments performed directly at the interface between wood cell walls and cured UF adhesive in the untreated reference and in silylated specimens showing different contact angles.

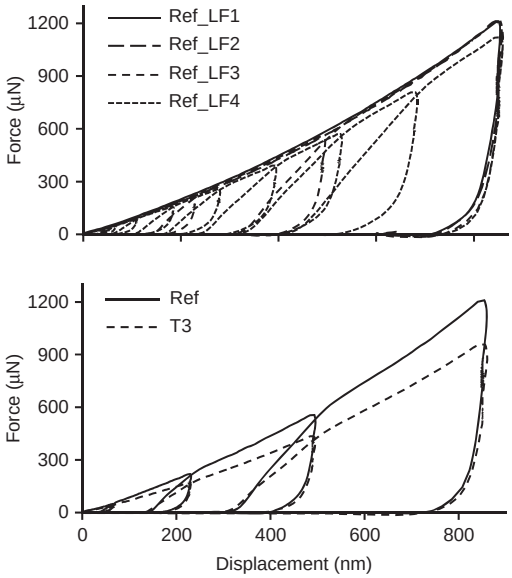

Figure 9 Mean force-displacement curves from NI experiments at the cell wall-adhesive interface using displacement controlled load functions. Top: comparison of results obtained on the reference sample using four different load functions; Bottom: comparison of results obtained on the reference and treated sample, respectively, using load function LF3. Specimen T3, which showed little macroscopic adhesion, required significantly less load to obtain the same indentation depth at the interface as the reference, indicating a weaker interface.

in Figure 6, which show no indication of changes in cell wall mechanics due to silylation. In contrast, the hardness at the interface decreases clearly with increasing CA (Figure 8). As the characterisation of pure cell wall and adhesive show no clear effect of silylation (Figure 6), it is proposed that the trend of decreasing hardness at the interface in parallel to an increasing CA (Figure 8) is related to variations in adhesion: decreasing adhesion at the cell wall-adhesive interface facilitates the penetration of the indenter body into the substrate. This statement agrees very well with the macroscopic trend of decreasing bond strength observed with increasing CA (Figure 5).

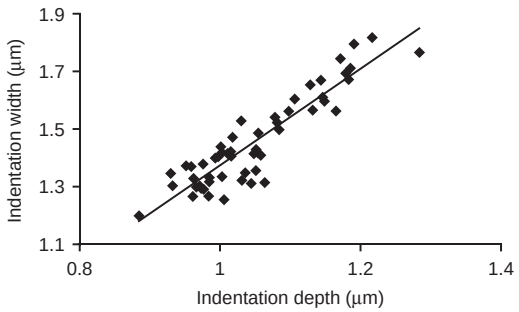

Figure 10 Linear relationship between the depth and the width of indents performed with a conical indenter directly at the interface between wood cell walls and UF adhesive.

Table 1 Average contact angle, macroscopic bond strength, and specific work of indentation for the differently treated samples (T1–T3) and load functions (force controlled and load controlled LF1–LF4 according to Figure 1), and the specific adhesive energy of the wood cell wall-UF interface calculated thereof.

			Specific work of indentation (J mm^{-2}) for				
				Displacement controlled NI			
Specimen	Contact angle (°)	Bond strength (MPa)	Force controlled NI	LF1	LF2	LF3	LF4
Reference	80	7.6	570±40	760±50	750±40	840±60	990±60
T1	102	5.3	560±30	–	–	–	–
T2	111	2.9	530±20	–	–	–	–
T3	135	0.2	490±30	700±90	640±80	720±120	820±240
Adhesive energy			80	60	110	120	170

Having thus established a relationship between the hardness at the interface and adhesion, a second set of experiments was performed in order to assess the influence of different load functions. Only the two most extreme samples, i.e., the untreated reference and the most severely hydrophobised OTS+CTMS treated samples were considered. The implementation of a force controlled load function results in varying NI depths, causing different deformation. To prevent this, at this step only displacement controlled load functions were chosen and the same deformation for all indents was afforded.

As visible in Figure 9, all four displacement-controlled load functions delivered similar results in terms of the maximum load reached at the target NI depth for reference samples. Comparing the reference and the OTS+CTMS hydrophobised sample, all load functions have a significantly lower peak force in treated samples. Figure 9 shows this difference for the example of load function 3. Thus the second set of indents demonstrates that less force is necessary to achieve a desired NI depth in the interface of treated specimens compared to the reference. Consequently, it can be safely concluded that the reduction in required force is due to the diminished adhesion at the interface.

As no evidence of extensive crack formation beyond the immediate indent was observed in AFM images (Figure 3), it can be assumed that debonding takes place essentially only in the immediate interface region penetrated by the conical indenter. The triangular debond region corresponding to the projected tip shape is defined by the known tip opening angle, by the maximum NI depth, and the NI width. While NI depth is automatically recorded, the NI width was determined from AFM images taken after experiments. Figure 10 shows a plot of NI widths compared to NI depth obtained in the force control mode.

A linear relationship is evident, which confirms that debond regions in different indents have the shape of geometrically similar triangles. The same was true for the displacement control mode, with a small deviation of the NI width around the mean. Based on this finding, the specific work of NI $\hat{W}_d$ can be estimated from the total work of NI W_d, the maximum indent depth h_{max}, and the constant c, giving the relation between NI width and NI depth, according to Eq. (1).

$$\hat{W}_d = c\frac{W_d}{\left(h_{\max}\right)^2} \tag{1}$$

The results of the calculation of the specific work of NI (Table 1) reveal a correlation with the type of treatment. As expected, the work of NI decreases with increasing CA and decreasing macroscopic bond strength of the samples, respectively. This effect is clear for both the force-controlled and the displacement-controlled modes. Due to the hysteretic behaviour for the latter mode (Figure 9), an increase in the specific work is found with an increasing number of unload-reload cycles. It is thus important not to change the load-function for a given experiment. As a consequence of the load-function dependence of the work of NI, the adhesive energy estimated from the difference between the reference and the OTS+CTMS treated sample is variable and ranges from 60 J mm^{-2} to 170 J mm^{-2} (Table 1).

It is therefore important to note that only relative comparisons of adhesion energy can be performed with this method, whereas more complex mathematical analysis will be required to extract absolute values. However, further information can be obtained from a comparison of relative values of specific work of NI, when values obtained for the reference sample are defined as 100%. Here, the decrease in the energy spent is in the order of 15% for all load functions with the only exception of the linear single-load function. It is suggested that the deviation of this load function results from the relatively high NI speed, which did not allow for proper delamination. From the difference in the work of NI between the well-bonded reference and the very weakly bonded OTS+CTMS sample for most load functions it can thus be concluded that in the presented experimental setup, 15% of the measured energy is due to adhesion at the interface.

Conclusion

It is possible to obtain an estimate of the specific adhesive energy between the wood cell wall and UF adhesive by means of nanoindentation (NI). While the absolute values vary clearly depending on procedural parameters, relative changes

remain constant and can provide valuable information about adhesive properties at the cell wall level when comparing differently treated samples. Further knowledge about the actual deformation and delamination processes could be probably helpful to improve the applicability of the presented method. NI is valuable in studying adhesion in ductile materials at the microscopic level.

Acknowledgments

Funded by the Austrian Science Fund (FWF): Project P21681-N22.

References

Clauss, S., Gabriel, J., Karbach, A., Matner, M., Niemz, P. (2011) Influence of the adhesive formulation on the mechanical properties and bonding performance of polyurethane prepolymers. Holzforschung 65:835–844.

de Meijer, M., Haemers, S., Cobben, W., Militz, H. (2000) Surface energy determinations of wood: Comparison of methods and wood species. Langmuir 16:9352–9359.

Drzal, L.T., Herrera-Franco, P.J., Ho, H. (2000) Fiber-matrix interfaces tests. Test methods, nondestructive evaluation and smart materials. In: Comprehensive Composite Materials. Eds. Kelly, A., Zweben, C. Elsevier, Amsterdam. Vol. 5, p.71.

Elizalde, M.R., Sánchez, J.M., Martínez-Esnaola, J.M., Pantuso, D., Scherban, T., Sun, B., Xuet, G. (2003) Interfacial fracture induced by cross-sectional nanoindentation in metal-ceramic thin film structures. Acta Mater. 51:4295–4305.

Gao, S.L., Mäder, E. (2002) Characterisation of interphase nanoscale property variations in glass fibre reinforced polypropylene and epoxy resin composites. Comp. Part A. 33:559–576.

Gaur, U., Miller, B. (1989) Microbond method for determination of the shear strength of a fibre/resin interface: evaluation of experimental parameters. Comp. Sci. Technol. 34:35–51.

Gindl, M., Tschegg, S.E. (2002) Significance of the acidity of wood to the surface free energy components of different wood species. Langmuir 18:3209–3212.

Gindl, W., Gupta, H.S., Schöberl, T., Lichtenegger, H.C., Fratzl, P. (1998) Mechanical properties of spruce wood cell walls by nanoindentation. Appl. Phys. A. 79:2069–2073.

Hansmann, C., Weichslberger, G., Gindl, W. (2005) A two-step modification treatment of solid wood by bulk modification and surface treatment. Wood Sci. Technol. 39:502–511.

Konnerth, J., Gindl, W., Harm, M., Müller, U. (2006) Comparing dry bond strength of spruce and beech wood glued with different adhesives by means of scarf- and lap joint testing method. Holz Roh. Werkst. 64:269–271.

Lee, S.H., Wang, S.Q., Endo, T., Kim, N.H. (2009) Visualization of interfacial zones in lyocell fiber-reinforced polypropylene composite by AFM contrast imaging based on phase and thermal conductivity measurements. Holzforschung 63:240–247.

Mohammed-Ziegler, I., Hórvölgyi, Z., Tóth, A., Forsling, W., Holmgren, A. (2006) Wettability and spectroscopic characterization of silylated wood samples. Polym. Adv. Technol. 17:932–939.

Molina-Aldareguia, J.M., Ocaña, I., González, D., Elizalde, M.R., Sánchez, J.M., Martínez-Esnaola, J.M., Gil-Sevillano, J., Scherban, T., Pantuso, D., Sun, B., Xu, G., Miner, B., He, J., Maiz, J. (2007) Adhesion studies in integrated circuit interconnect structures. Eng. Failure Anal. 14:349–354.

Oliver, W.C., Pharr, G.M. (1992) Improved technique for determining hardness and elastic modulus using load and displacement sensing indentation experiments. J. Mater. Res. 7:1564–1580.

Peterlin, S., Planinsek, O., Moutinho, I., Ferreira, P., Dolenc, D. (2010) Inverse gas chromatography analysis of spruce fibers with different lignin content. Cellulose 17:1095–1102.

Roy, S., Darque-Ceretti, E., Felder, E., Monchoix, H. (2007) Cross-sectional nanoindentation for copper adhesion characterization in blanket and patterned interconnect structures: Experiments and three-dimensional FEM modelling. Int. J. Fracture 144: 21–33.

Sahaf, A., Englund, K., Laborie, M.P.G. (2012) Tack and shear strength of hybrid adhesive systems made of phenol-formaldehyde, dextrin and fish glue, and acrylic pressure-sensitive adhesive. Holzforschung 66:73–78.

Sánchez, J.M., El-Mansy, S., Sun, B., Scherban, Z., Fang, N., Pantuso, D., Ford, W., Elizalde, M.R., Martiñez-Esnaola, J.M., Martiń-Meizoso, A., Gil-Sevillano, J., Fuentes, M., Maiz, J. (1999) Cross-sectional nanoindentation: A new technique for thin film interfacial adhesion characterization. Acta Mater. 47:4405–4413.

Scheikl, M., Dunky, M. (1998) Measurement of dynamic and static contact angles on wood for the determination of its surface tension and the penetration of liquids into the wood surface. Holzforschung 52:89–94.

Singh, H.K., Chakraborty, A., Frazier, C.E., Dillard, D.A. (2010) Mixed mode fracture testing of adhesively bonded wood specimens using a dual actuator load frame. Holzforschung 64:353–361.

Zhandarov, S., Mäder, E. (2005) Characterization of fiber/matrix interface strength: Applicability of different tests, approaches and parameters. Comp. Sci. Technol. 65:149–160.

Received October 10, 2011. Accepted January 31, 2012.
Previously published online February 29, 2012.

Paper 2 - Evaluating Fundamental Position-Dependent Differences in Wood Cell Wall Adhesion Using Nanoindentation

International Journal of Adhesion & Adhesives 40 (2013) 129–134

Contents lists available at SciVerse ScienceDirect

International Journal of Adhesion & Adhesives

journal homepage: www.elsevier.com/locate/ijadhadh

Evaluating fundamental position-dependent differences in wood cell wall adhesion using nanoindentation

Michael Obersriebnig *, Johannes Konnerth, Wolfgang Gindl-Altmutter

Department of Materials Science and Process Engineering, BOKU-University of Natural Resources and Life Science, Konrad Lorenz Strasse 24, A-3430 Tulln, Vienna, Austria

ARTICLE INFO

Article history:
Accepted 15 August 2012
Available online 29 August 2012

Keywords:
Adhesives for wood
Interfaces
Dynamic mechanical analysis
Wood

ABSTRACT

Spruce wood specimens were bonded with one-component polyurethane (PUR) and urea-formaldehyde (UF) adhesive, respectively. The adhesion of the adhesives to the wood cell wall was evaluated at two different locations by means of a new micromechanical assay based on nanoindentation. One location tested corresponded to the interface between the adhesive and the natural inner cell wall surface of the secondary cell wall layer 3 (S3), whereas the second location corresponded to the interface between the adhesive and the freshly cut secondary cell wall layer 2 (S2). Overall, a trend towards reduced cell wall adhesion was found for PUR compared to UF. Position-resolved examination revealed excellent adhesion of UF to freshly cut cell walls (S2) but significantly diminished adhesion to the inner cell wall surface (S3). In contrast, PUR showed better adhesion to the inner cell wall surface and less adhesion to freshly cut cell walls. Atomic force microscopy revealed a less polar character for the inner cell wall surface (S3) compared to freshly cut cell walls (S2). It is proposed that differences in the polarity of the used adhesives and the surface chemistry of the two cell wall surfaces examined account for the observed trends.

1. Introduction

The mechanical characterisation of adhesion is of utmost importance in order to evaluate differences in the performance of adhesives. On the one hand, mechanical experiments can be performed in a relatively straightforward manner with comparably homogeneous materials such as metals or polymers. On the other hand, the mechanical characterisation of adhesion in a heterogeneous, porous, and hierarchically structured material like wood poses a serious challenge with regard to the correct interpretation of results. Current testing standards such as [1] and similar international standards rely predominantly on shear testing (lap-shear or block-shear) and delamination testing with and without pre-treatment by moisture, heat, and combinations thereof. In an application-oriented context, these methods deliver useful and reliable results on adhesive performance. However, in a more scientific context, results obtained using standardised tests are often difficult to interpret due to the complex microstructure of the involved material (e.g. [2]). In particular, the nature of the interface between wood and an adhesive, which consists of neat adhesive and neat wood, and a zone where wood and adhesive interpenetrate, makes it difficult to track down the point of initiation of failure. In an effort to obtain information on the practical adhesion directly at the interface between the wood cell wall and an adhesive polymer and thus avoiding effects originating from surface roughness and adhesive penetration at the micron-scale, a modified nanoindentation test was introduced recently [3]. It was demonstrated that the total energy spent in an indentation experiment directly at the interface between the wood cell wall and urea-formaldehyde adhesive was related to the strength of adhesion between the two partners, i.e. the required indentation energy increased with increasing adhesive bond strength. In the present study, this new micromechanical assay is used to investigate the adhesion of one-component polyurethane (PUR) and urea-formaldehyde-based adhesive (UF), to wood surfaces on the cell wall level.

PUR and UF belong to two groups of wood adhesives which differ significantly in their chemistry, structure-property and wood–adhesive interaction relationships [4]. PUR may be classified as pre-polymerised adhesive with large average molecular weight components. However, depending on the specific type of PUR, a wide distribution of properties is possible [5]. UF on the other hand belongs to the group of in-situ polymerised adhesives. It is characterised by a broad distribution of molecular weight fractions, high hydrophilicity and ability to penetrate into the wood cell wall, resulting in significantly altered mechanics of cell walls next to the adhesive [6–8]. In its cured state, PUR usually is comparably soft and ductile, whereas UF may be characterised as

* Corresponding author. Tel.: +43 1 47654 4290; fax: +43 1 47654 4295.
E-mail address: m.obersriebnig@boku.ac.at (M. Obersriebnig).

0143-7496/$ - see front matter © 2012 Elsevier Ltd. All rights reserved.
http://dx.doi.org/10.1016/j.ijadhadh.2012.08.011

hard and brittle [9]. The strong interpenetration between wood and adhesive both at the cell-cavity and the cell-wall scales typical of in-situ polymerised resins such as UF results in a dominance of cohesive failure in neat wood next to the bond line (wood failure, Fig. 1). Since in this case the adhesive bond line appears to be stronger than solid wood, a high proportion of wood failure is considered an indicator for high bond durability. In this context, the failure pattern of most PURs differs significantly, since the percentage of wood failure is often low (Fig. 1), specifically after moisture treatment, even if a high shear strength is retained [10].

Applying a newly developed micromechanical assay the present study aims at obtaining new information on the interaction of PUR and the wood cell wall compared to UF. Results of such experiments are expected to help with interpretation of the particular behaviour of PUR in the adhesive bonding of wood. As the main aim is the application and presentation of the method rather than giving a full presentation of differing properties of adhesives, only one commercially available PUR- and UF-adhesive is tested, respectively, and only on spruce wood samples.

2. Materials and methods

2.1. Sample preparation

Norway spruce (*Picea abies*) samples from different parts in the stem were impregnated with water for several days in order to soften them prior to microtoming. By means of a conventional sledge microtome equipped with a steel knife, a smooth surface was cut along the tangential anatomical plane parallel to the direction of wood fibres. After that, samples were dried and stored in standard climate for several days before they were bonded with a one-component polyurethane adhesive (PUR, Purbond HB S309, Purbond AG, Switzerland) and urea-formaldehyde-based adhesive (UF, W-Leim Spezial, Dynea, Austria), respectively. After curing at ambient conditions, nanoindentation (NI) specimens were prepared from small pieces of wood containing the adhesive bond line. Cross sections normal to the direction of wood fibres were cut without prior embedding in epoxy resin using a diamond knife on an ultramicrotome (Leica) to provide smooth indentation surfaces. During each step of sample manipulation, special care was given to the fibre orientation in order to ensure that the final plane of indentation was normal to the fibre direction.

2.2. Nanoindentation

All NI experiments were performed on a Hysitron nanoindenter using a cone shaped diamond tip with a total opening angle of 60° and a tip radius of 10 nm. As load function, a linear four-step displacement controlled function with a quadratic increase of peak displacement from step to step and partial unloading after each step to half peak displacement was chosen as it yielded the best results in a comparison of various load functions. The implementation of load–partial unload cycles slows down the indentation process, thus allowing for deformation to follow the path of least resistance while still allowing for relatively fast indentation speed so as to reduce creep deformation during the load phase. Displacement control is necessary to provide the same total deformation for all samples, therefore giving a means of comparing indentation energies. Indents were performed at the interface between the adhesive and the wood cell wall at positions shown in Fig. 2. A first set of indents was taken at the (natural) inner surface of the cell wall (P1), corresponding to the secondary cell wall layer 3 (S3). A second set was performed at the (artificial) surface created by cutting through the cell wall in the process of surface preparation (P2). This surface corresponds to the cut-open surface of the secondary cell wall layer 2 (S2). The precise positioning of indents was performed on 15 μm × 15 μm scanning probe micrographs taken with the indenter tip. For all indents, care was taken that in an area of approximately 5 μm radius no pre-damage, be it from sample preparation or other indents, was visible. The indentation energy for each indent was calculated as the numeric integral of the force–displacement curves (F–d curves). As demonstrated in [3], the principle underlying the evaluation of indentation energy is that there is a contribution of adhesion to the total indentation energy at the cell wall–adhesive interface. Thus e.g. diminishing adhesion will result in diminishing total indentation energy.

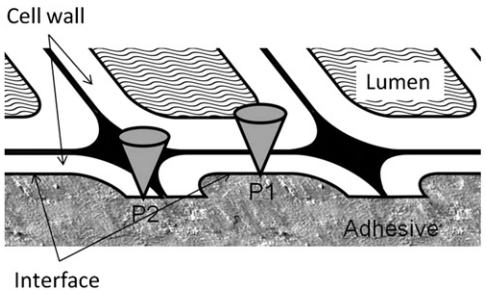

Fig. 2. Schematic representation of indent positions at the cell wall–adhesive interface. Position 1 (P1) is located at the natural inner surface of the cell cavity. Position 2 (P2) is located at the artificial cell wall surface cut-open in the process of wood surface preparation. To prevent artefacts, indents were only performed in areas of at least 5 μm radius without visible damage or further interfaces. This implicates that only latewood cells were tested.

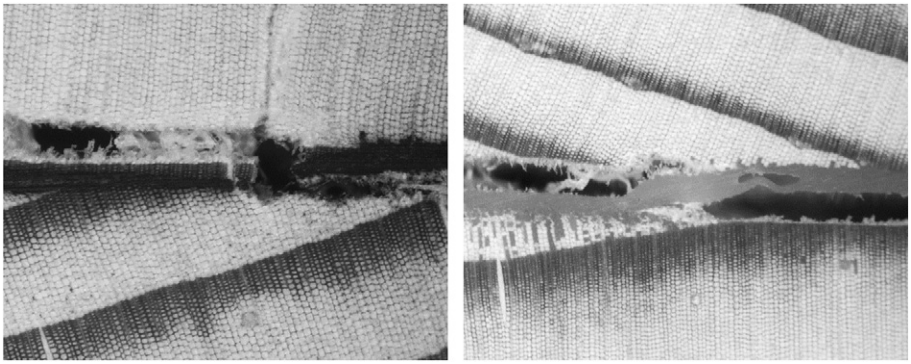

Fig. 1. Typical patterns of bond line failure in delamination testing. Left: failure occurs in neat wood next to the bond line (cohesive wood failure). Right: failure occurs by delamination between wood and adhesive (adhesion failure).

2.3. Atomic force microscopy (AFM)

In order to obtain additional information on the processes taking place during an indentation experiment at the wood cell wall–adhesive interface, in particular the eventual formation of cracks, a number of residual indents in both UF- and PUR-bonded samples were scanned with an AFM one day after indenting. All images were taken on a Dimension Icon AFM (Bruker, Santa Barbara, CA) in tapping mode. The tips were mounted on standard silicon cantilevers with a resonance frequency of 330–340 kHz and a nominal tip radius of less than 12 nm. Images taken were 2 μm in size with a standard drive frequency of 0.7 lines per second. Gain factors and amplitude settings were adjusted for each scan but were of comparable values for all scans. Using software provided by the manufacturer, topography images were inverted for easier viewing and x–z-data parallel and normal to the bond line through the indent peak was analysed in order to obtain characteristic indent profiles.

With the aim of characterising possible differences in the polarity of the cell wall surface at the two indentation positions (P1 and P2 according to Fig. 2) chosen, chemical force microscopy was performed using untreated silicon tips on a silicon nitride cantilever. The system measures the adhesion by performing small indents at every point of the scan and evaluating the load–unload curves. The force required to detach the tip from the indented surface corresponds to adhesion and depends on the surface chemical characteristics of the surface and the tip, respectively. Indent depths varied between 30 nm and 50 nm with scan rates ranging from 0.5 to 1 Hz. The cantilever stiffness was measured by thermal tuning and was about 0.4–0.5 N/m for varying tips. The nominal tip radius was 2 nm, however it was not known or measured exactly which is why results were evaluated only qualitatively. To obtain a qualitative evaluation of the tip polarity, a model system consisting of a lyocell fibre (100% cellulose, polar) embedded in epoxy (unpolar) was scanned with the same settings.

3. Results and discussion

3.1. Comparison of PUR and UF

The results of indentation experiments are shown as representative mean F–d curves in Fig. 3. Overall, a much higher peak force is required to reach a desired displacement with UF than with PUR. This significant difference may be well explained by the higher stiffness of the UF as compared to the PUR [9] and the penetration of the UF into the cell wall [6], leading to an effectively increased stiffness of the total cell wall–adhesive system. It is thus proposed that the composite cell wall–UF poses more resistance towards indentation compared to the cell wall–PUR composite.

It is an important prerequisite for the determination of adhesive energy using the present method that the stiffness of the systems considered remains unchanged [3]. Due to the clear difference in stiffness by a factor in the order of 10 between UF and PUR [9], it is not possible to draw global conclusions on eventual differences in adhesion between wood and UF or PUR, respectively, from results shown in Fig. 3, however, an inspection of residual indents from experiments performed at the cell wall–adhesive interface by means of AFM (Figs. 4 and 5) reveals small differences in indent geometry which may be interpreted in terms of adhesion. Indents at the cell wall–UF interface shown in Fig. 4 nicely depict the geometry of the conical indenter. The profile of the indent peak is the same regardless whether a section parallel or normal to the

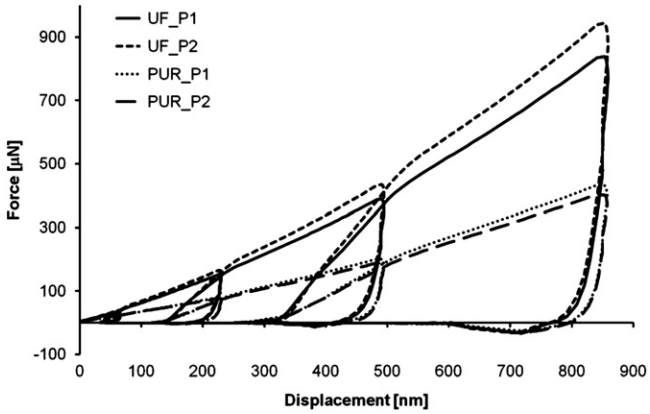

Fig. 3. Mean force–displacement (F–d) curves for all indent series. While the target displacement is the same for all sets of indents, significantly different force was required to achieve the desired displacement.

interface is considered. This may be interpreted as a sign of relatively good adhesion, since a similar amount of plastic deformation has occurred parallel to the interface and also normal to it. In contrast, this symmetry is not observed in indents at the cell wall–PUR interface (Fig. 5). Here, the residual indent peak is significantly wider and less sharp parallel to the interface than normal to it. The asymmetry in the profile normal to the interface shown in Fig. 5a can be explained by the slight displacement of the indent towards the adhesive. The indent eventually reaches the interface and leads to delamination as well as the asymmetry. However, such slight misplacements were not found to lead to significant deviations in the work of indentation. It remains true that the actual indent peak however is much sharper normal to the interface than parallel to it, indicating that plastic deformation more easily takes place along the interface than transverse to it. It seems that the interface is a point of weakness in the system cell wall–PUR, which is apparently not in the system cell wall–UF. This may be attributed to the penetration of the UF into the cell wall [6], leading to a more homogenous mechanical system with a less well defined interface. In terms of adhesion one may conclude that overall the direct interfacial adhesion to wood is weaker for PUR than for UF. Of course, this may not necessarily translate to reduced macroscopic bond durability, since the latter is a result of additional factors such as e.g. effects of surface roughness and cell lumen or cell-wall penetration [4]. At least, the lack of wood failure observed for PUR in certain testing regimes [10] may have its origin in a measurable weakness of adhesion at the interface with the cell wall.

3.2. Comparison of adhesion to the natural inner cell wall surface (S3) and to cut-open cell walls (S2)

While the discussion of eventual differences in the adhesion between the cell wall and PUR or UF, respectively, has to rely only on the geometry of residual indents, the results presented in Figs. 3 and 6 allow to draw more straightforward and quantitative conclusions on differences in adhesion of these two adhesives to the cell wall surface types P1 and P2 examined in the present study. When UF is used for adhesive bonding, a higher peak force is required to achieve the target indentation displacement at P2, i.e. the freshly cut surface through the cell wall S2, compared to P1 located at the natural inner surface of the cell lumen (S3). Surprisingly, the opposite trend is found for the PUR-adhesive, where a higher force is required at P2 compared to P1.

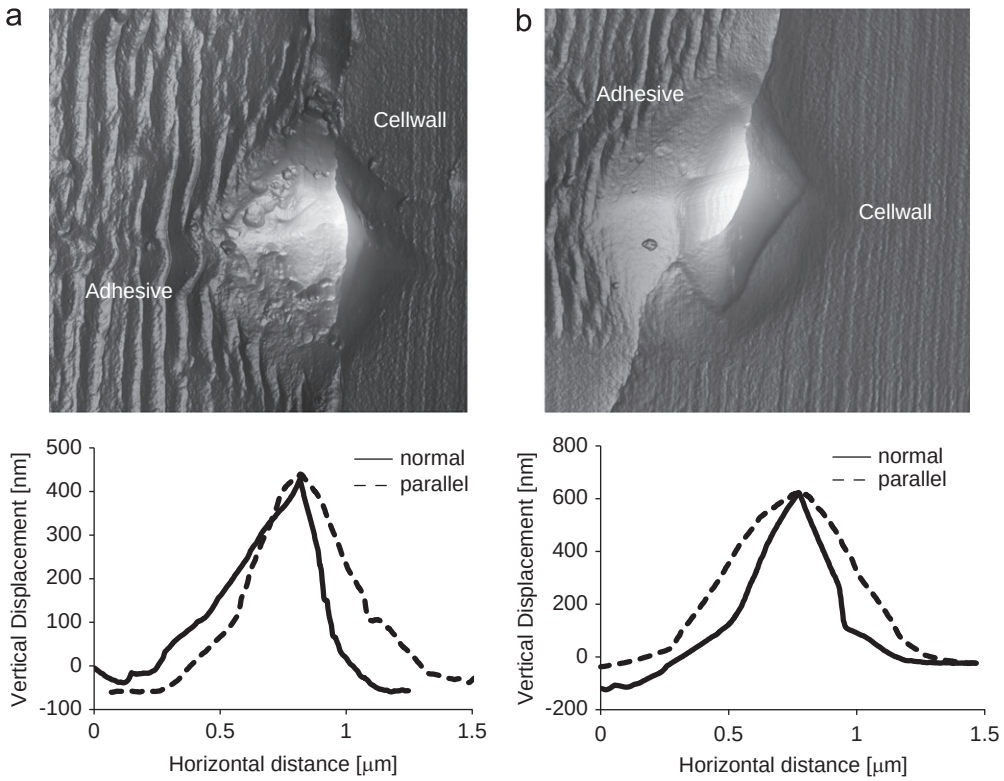

Fig. 4. Inverted AFM-scans of interfacial indents on the UF-bonded sample (above) at P2 (a) and P1 (b). Section data was taken normal and parallel to the bond line at the indent peak (below).

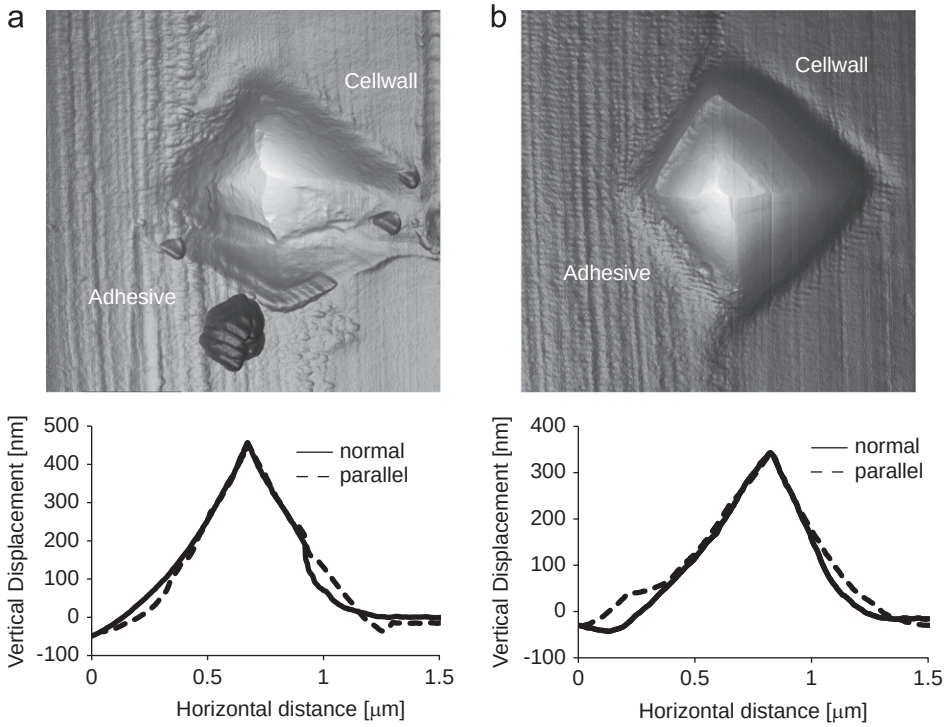

Fig. 5. Inverted AFM-scans of interfacial indents on the PUR-bonded sample (above) at P2 (a) and P1 (b). Section data was taken normal and parallel to the bond line at the indent peak (below).

In accordance with the information from the mean F–d curves, the indentation energy obtained by numerical integration of the curves (Fig. 6) shows a highly significant increase ($\alpha < 0.001$) of approximately 10.4% for P2 indents on the UF-bonded sample as compared to P1-indents. For PUR-bonded samples, the variation is smaller but still significant with a 4.9% decrease of indentation work for the P1-indents compared to P2 ($\alpha < 0.01$). Considering Fig. 6 the difference in indentation work between P1 and P2

seems small at first view, but this impression is misleading. The indentation work shown in Fig. 6 is the sum of work spent for deforming the cell wall and the adhesive, and for separating the adhesive from the cell wall. For the indentation settings used in the present study, Obersriebing et al. [3] found that in a well bonded UF specimen the contribution of adhesion to the total indentation work is in the order of 15%. Therefore a difference of indentation work of+10.4% corresponds roughly to a change in adhesion in the order of+60%. The decrease in indentation work of 4.9% for the PUR bonded specimen would in that aspect indicate decreased adhesion strength of about 30%. However, it is at least doubtful if the contribution of work of adhesion to the total indentation work can be compared for these very different mechanical systems. Still, these remarkable values indicate significant differences in the chemistry of the cell wall surfaces at the two positions examined in the present study. It is well known that the hydrophilicity of a wood surface is highest when it is freshly cut, and decreases with increasing age of the surface [11]. With regard to the cell wall surfaces at P1 and P2 examined in the present study, results from chemical force microscopy support the assumption of different surface chemistry. The scan on the model system epoxy–lyocell, i.e. a less hydrophilic and a more hydrophilic surface, clearly shows better adhesion on the lyocell cross section for the AFM tip used in this experiment (Fig. 7a). Thus Fig. 7a indicates that the tip is sensitive to changes in surface polarity, showing higher adhesion to more polar surfaces. Several scans performed on the edge of cut open cells on the tangential section, containing the S2 and S3 layer of the cell wall, all showed better adhesion on the S2 layer (Fig. 7b and c), confirming its higher polarity as compared with the inner cell wall layer. This is even more notable as the sections were already a few days old, allowing the S2-layer time to age and lose some of its polarity. However, as can be seen in Fig. 7c, the variation between S2 and S3 is also clearly visible for the cut-open part of the S3-layer. This indicates different chemical properties not only at the (aged) surface but in the cell wall bulk. Thus one might assume that the cut-open surface present at P2 (Fig. 2) is more hydrophilic than the lumen surface at P1. On the other hand, liquid UF has a pronounced hydrophilic character due to its high content of water and abundance of accessible—OH groups [12] whereas the chemical structure of PUR [13] indicates much less pronounced hydrophilicity. Considering the different character of the two adhesives in terms of different degrees of hydrophilicity used in the present experiment, better adhesion of UF to P2 may be expected compared to P1, whereas the opposite is the case for PUR in agreement with the results presented in Fig. 6. Of course, it has to be mentioned that other properties, like the surface roughness or the indentation rate may influence the measured values of adhesive strength. However, it was found in a previous unpublished experiment that the roughness seems to have no significant influence on the outcome of this test compared to that of the surface polarity. The same is true for the indentation rate concerning the relative values of indentation energy, as long as the rate is kept below a threshold value. It is thus concluded that the observed differences in cell-wall surface chemistry are responsible for the differences in cell-wall adhesion measured with UF and PUR, respectively, in the present study.

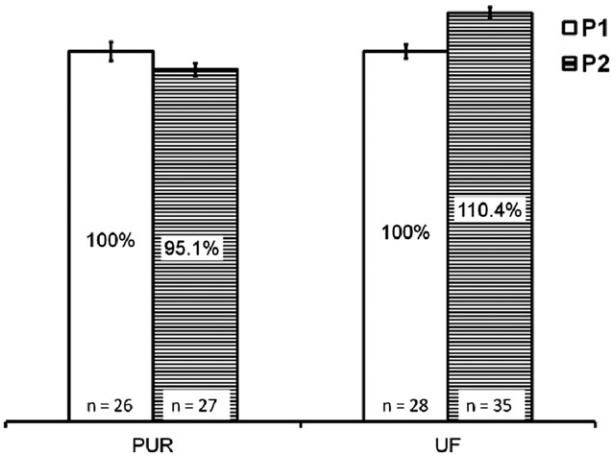

Fig. 6. Mean relative indentation work. The higher value is defined as 100%, the error bars represent the α=0.01 confidence intervals of the mean. n=number of indents performed for the sample type.

4. Conclusion

The results obtained in this study are of significance from two points of view. On the one hand, they demonstrate that the morphology of residual indents at the cell wall–adhesive interface delivers valuable qualitative information on the strength of adhesion. Clear indications were found that overall the interface between the wood call wall and PUR is weaker than the interface between the cell wall and UF. This can presumably be attributed to the penetration of UF into the cell wall. On the other hand, quantitative analysis of indentation curves at the interface demonstrated that the pattern of interaction between the cell wall and the adhesives PUR and UF differs fundamentally. While UF shows better adhesion to the more hydrophilic S2-layer of the cell wall and less adhesion to the natural inner cell wall surface (S3), PUR shows the opposite trend. The overall clarity of the results demonstrates the usefulness of this nanoindentation-based method for wood science and research on wood adhesion, e.g. evaluating the influence of different curing properties (temperature, humidity) on the final adhesive strength.

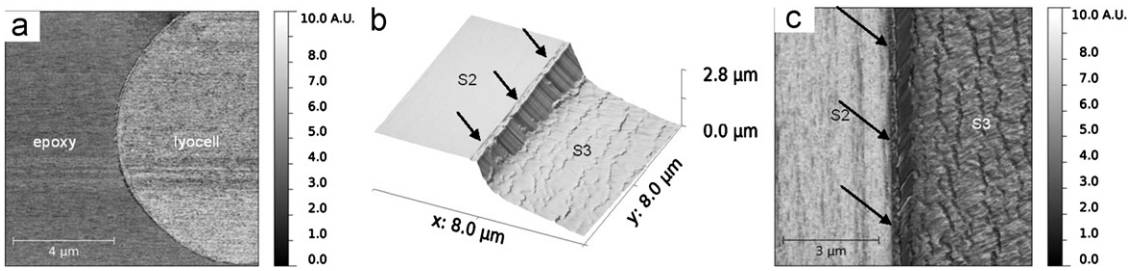

Fig. 7. Selected AFM scan images. (a) Chemical force micrograph taken on a model lyocell–epoxy system, showing better adhesion (lighter colour) on the polar lyocell cross section. (b) Topography image at the edge of a cut open cell, showing the S2 and S3 layer of the cell wall. (c) Chemical force micrograph at the same position, showing better adhesion on the S2 layer, thus indicating its higher hydrophilicity; arrows indicate the cut-open part of the S3-layer in images b and c.

Acknowledgement

Funded by the Austrian Science Fund FWF: Project No. P21681.

References

[1] EN 302. Adhesives for load-bearing timber structures—Test methods; 2004.
[2] Frihart CR. Adhesive bonding and performance testing of bonded wood products. J ASTM Int 2005;2 JAI12952.
[3] Obersriebnig M, Veigel S, Gindl-Altmutter W, Konnerth J. Direct evaluation of adhesive energy at the wood cell-wall urea-formaldehyde interface using nanoindentation technique. Holzforschung, in press.
[4] Frihart CR. Adhesive groups and how they relate to the durability of bonded wood. J Adhes Sci Technol 2009;23:601–17.
[5] Beaud F, Niemz P, Pizzi A. Structure-properties relationships in one component polyurethane adhesives for wood: sensitivity to low moisture content. J Appl Polym Sci 2006:4181–92.
[6] Konnerth J, Harper D, Lee SH, Rials TG, Gindl W. Adhesive penetration of wood cell walls investigated by scanning thermal microscopy (SThM). Holzforsch 2008;62:91–8.
[7] Gindl W, Gupta H. Cell-wall hardness and Young's modulus of melamine-modified spruce wood by nano-indentation. Compos A 2002;33:1141–5.
[8] Stöckel F, Konnerth J, Kantner W, Moser J, Gindl W. Tensile shear strength of UF- and MUF-bonded veneer related to data of adhesives and cell walls measured by nanoindentation. Holzforsch 2010;64:337–42.
[9] Konnerth J, Jäger A, Eberhardsteiner J, Müller U, Gindl W. Elastic properties of adhesive polymers. II. Polymer films and bond lines by means of nanoindentation. J Appl Polym Sci. 2006;102:1234–9.
[10] Vick CB, Okkonen EA. Strength and durability of one-part polyurethane adhesive bonds to wood. For Prod J 1998;48:71–6.
[11] Gindl M, Reiterer A, Sinn G, Stanzl-Tschegg SE. Effects of surface ageing on wettability, surface chemistry, and adhesion of wood. Holz Roh Werkstoff 2004;62:273–80.
[12] Scheikl M, Dunky M. Measurement of dynamic and static contact angles on wood for the determination of its surface tension and the penetration of liquids into the wood surface. Holzforschung 1998;52:89–94.
[13] Clauß S, Dijkstra DJ, Gabriel J, Kläusler O, Matner M, Meckel W, et al. Influence of the chemical structure of PUR prepolymers on thermal stability. Int. J. Adhes Adhes 2011;31:513–23.

Paper 3 - The Optical Appearance of Wood Related to Nanoscale Surface Roughness

The Optical Appearance of Wood Related to Nanoscale Surface Roughness

Markus Hauptmann,[a,*] Ulrich Müller,[b] Michael Obersriebnig,[b] Wolfgang Gindl-Altmutter,[b] Adrian Beck,[c] and Christian Hansmann [a]

The color and appearance of timber is influenced by a variety of physical and chemical effects. Especially the chemical composition and the surface structure play a major role. In particular, the influence of chromophore extractives and the effect of thermal degradation processes on the color of wood are widely discussed in the literature. The present study deals with the influence of the surface nanostructure on the visual appearance of wood. This new perspective should generally demonstrate various influences on the appearance of natural inhomogeneous surfaces. Therefore, two methods were used to change the nanoroughness of lignocellulose materials. With different oil coatings and UV-irradiation, the surface structures of the samples were changed, and the measured roughness using atomic force microscopy was then correlated with the collected brightness differences. The results show that a clear correlation exists between the nanoroughness altered by oil coatings or UV irradiation and the brightness of the wood surface. Due to various other influences, such as chemical changes and light refractions of the treated wood structure which also influence the color of wood, no quantification can be given at this point.

Keywords: Appearance; Color; Gloss; Nano; Roughness; Wood

*Contact information: a: Wood K plus –Kompetenzzentrum Holz GmbH, Altenberger Strasse 69, A-4040 Linz, Austria; b: University of Natural Resources and Life Sciences, Department of Material Sciences and Process Engineering, Vienna, Austria; c: Team7 Natürlich Wohnen GmbH, Braunauer Str. 26, A-4910 Ried im Innkreis, Austria; *Corresponding author: m.hauptmann@kplus-wood.at*

INTRODUCTION

Wood is widely used as a diverse building material, not only because of its mechanical properties, but also for its aesthetic appearance. The color and the contrast of wood surfaces are thus of great interest for wood science in order to explain or influence different color phenomena.

The color of wood is formed by the specific reflection or absorption of light waves of a spectrum. This leads to a variety of relevant optical effects, which all form the resulting appearance. The absorption of light on wood surfaces was studied by Vorreiter (1949) and Norrstrom (1969). They examined the specific absorption of the different macromolecules and extractives in wood. According to their work, lignin is responsible for the greatest part of light absorption. Depending on the wood species, lignin is responsible for 80 to 95% of the overall light absorption in wood. In comparison, carbohydrates are only responsible for 5 to 20% of the absorption and reflect most of the incoming light. Gierlinger *et al*. (2004) showed in their work that variations of extractives and phenolic compounds have an influence on the color of larch wood. This was also found later by Moya *et al*. (2012) for *Acacia mangium* and *Vochysia guatemalensis* wood.

The absorption of light by the irradiated wood defines not only its appearance, but also the specific reflections on its surface. Hence, the variation in the overall appearance of different wood species cannot only be explained due to the variation of the chemical composition. The specific reflections are also influenced by the roughness of the irradiated surface, which is therefore an important factor for the appearance of an object (de la Rie 1987). The gloss, as well as the color saturation, is influenced by the roughness (de la Rie 1987). On a rough surface, light is not only specularly reflected, but also diffused. Scattered light from a rough surface appears whiter (the reflection spectrum in the reflection minimum increases). Consequently, the appearing color will be desaturated (de la Rie 1987). This effect is most noticeable in darker areas because there is a higher proportion of scattered light (de la Rie 1987). In addition, the work of Watanabe *et al*. (2007) showed that roughness values, as obtained with an atomic force microscope (AFM), allowing height differences of less than 1 nm to be measured, have an influence on the apparent color of an object.

For investigations of surface properties on wood, the atomic force microscope is widely used (Tshabalala *et al.* 2003). The roughness (Meincken and Evans 2009) and also the hardness (Gindl *et al*. 2002) and chemical properties of cellular solids (Koljonen *et al*. 2003) can be analyzed.

The influences that lead to color changes on wood are of scientific and also of industrial interest. Studies providing analysis of the relationship between color changes of wood and structural changes at the nano level were not found in the literature. Therefore, the present work examines the influence of the surface roughness on the appearance of wood. Specifically, the brightness difference due to the various rough surfaces was analyzed.

MATERIALS AND METHODS

To study the appearance of wood depending on its roughness, the roughness of lignocellulose materials was altered using two different methods.

Oil Coatings

In the first method, the wood surface was altered by thin oil coatings. The resulting changes in color and brightness were then correlated with the measured structure.

For these thin coatings, commercially available walnut oil, linseed oil, sunflower oil, and castor oil were used. All of the oils were able to crosslink and thereby form a stable structure. Prior to the application, the oils were boiled for one hour to ensure a faster hardening of the coatings. They were then applied on ten 120x60x4 mm oak wood (*Quercus robur*) lamellae, which were ground in advance with a grain size of 220 µm. For each sample, 135 g/m² of oil was applied to the wood surface with a pipette and consequently spread with a fresh paper towel to provide a uniform distribution.

The color of the wood was measured three times per sample using a Chroma Meter CR-410 (Konica Minolta, Tokyo, Japan), with a measuring diameter of 50 mm and a D65 light source in a 2° observer angle. To calculate the color differences, the CIELAB system was used (DIN 6174 1979). In the CIELAB system, the L axis represents the brightness (L varies from 100 for white to zero for black), and a and b are the chromaticity coordinates ($+a$ for red, $-a$ for green, $+b$ for yellow, $-b$ for blue) (DIN 6174

1979). Because no major chroma changes due to structural differences are known from the literature, only the brightness change was investigated. The specific brightness differences were calculated as follows,

$$\Delta L = \sqrt{(L_1 - L_2)^2} \quad (1)$$

where the indices stand for the color of the treated sample (1) and untreated sample (2).

An atomic force microscope was used to measure the roughness of the oil-coated samples. Because it was not possible to perform AFM scans on solid wood due to the macroroughness, coated Typha fibers (*Typha latifolia*) were used as an alternative. To defibrate the *Typha* plants, three trunks were disintegrated with a razor blade. The individual fibers were then removed using a forceps. The Typha fiber provided a relatively large surface without any major cavities, but it is also a lignocellulosic material like wood. Three fibers were dipped into the oil and then placed on a paper towel; therefore the surplus oil could drain off the fiber. After that, the fibers were conditioned (20 °C/65% RH) for a period of two weeks. To select appropriate measurement points for the AFM, electron microscopy (Quanta 250 FEG, FEI, Hillsboro, OR, USA) was used. Spots with a similar surface structure were chosen for every used fiber. The following AFM measurements were performed on a Bruker Dimension Icon (Bruker, Santa Barbara, CA, US) in standard tapping mode. The tip, from the same manufacturer, had a nominal tip radius of < 10 nm. The scanning frequency was 1 Hz for all of the scans. An image analysis was performed using the Gwyddion 2.26 software. For each coating, three positions were scanned. Nanoroughness was measured with 50 points per data record at the same area where the color was measured and represented as a mean. The nanoroughness (R_n) of the different data points was calculated as follows,

$$R_n = \frac{1}{l}\int_0^l |y(x)|dx \quad (2)$$

where y is the deviation from the mean of the profile and l is the reference distance.

UV-Irradiation

In the second method employed to verify the influence of roughness parameters on the appearance of wood, maple wood (*Acer pseudoplatanus*) was irradiated with UV-light. Because much more extractive materials are included in oak and thus potentially more chemical processes occur, the wood species was changed to maple. Two thin sections of maple wood with a thickness of 30 µm were prepared with a microtome. The thin sections were irradiated in four steps, for 1, 2, 4, and 8 h, according to ISO 4892-2 Cycle 6 (2013). In the beginning and after every step, the color and the surface roughness of a specific point on the sample using AFM were measured. The color measurements were performed with a Phyma Codec 400 Vis spectrometer (Gaaden, Austria). The reflection spectrum was acquired from a measuring spot of 12 mm in the 400 to 700 nm region. The color parameters were calculated using the CIELAB system (DIN 6174 1979).

The AFM measurements on the thin sections were measured and analyzed, similar to the process used with the oil-coated fibers. The AFM measurements were performed on three spots after each irradiation step. Care was taken to scan approximately the same position after each step.

Using Fourier transform infrared spectroscopy (FTIR), the thin sections were measured after each step to analyze chemical changes in the tested areas. The samples were measured using an Attenuated Total Reflection (ATR) device (Helios, with a diamond crystal) and a Tensor 27 (Bruker Optics GmbH) spectrometer measuring a spectral range between 4000 cm^{-1} and 400 cm^{-1} with a spectral resolution of 4 cm^{-1} and 8 scans per spectra. Each wood sample was measured four times after each irradiating step, and the averages of the spectra were used for the analysis. A baseline correction with the rubber band method was applied with the software package Opus (Version 6) from Bruker. To determine in more detail the chemical degradation, the ratio between the lignin (1505 cm^{-1}) and the carbohydrates (1375 cm^{-1}), as well as the ratio of the carbonyl (1734 cm^{-1}) to the carbohydrates, was calculated (Pandey 2005). The carbohydrate peak at 1375 cm^{-1} was not affected by irradiation and was therefore used as a reference. Hereinafter, the maximum heights of the specific peaks at 1505 cm^{-1}, 1375 cm^{-1}, and 1734 cm^{-1} were measured and divided.

RESULTS AND DISCUSSION

The color measurements of the oil-coated lamella showed clear differences between the different surface treatments (Fig. 1). Also, a variation in the nanoroughness of the fibers measured with the AFM was found for the different oil treatments. Figure 1 shows a clear relation between the nanoroughness of the fibers and the brightness change of the coated wood (R^2= 0.93).

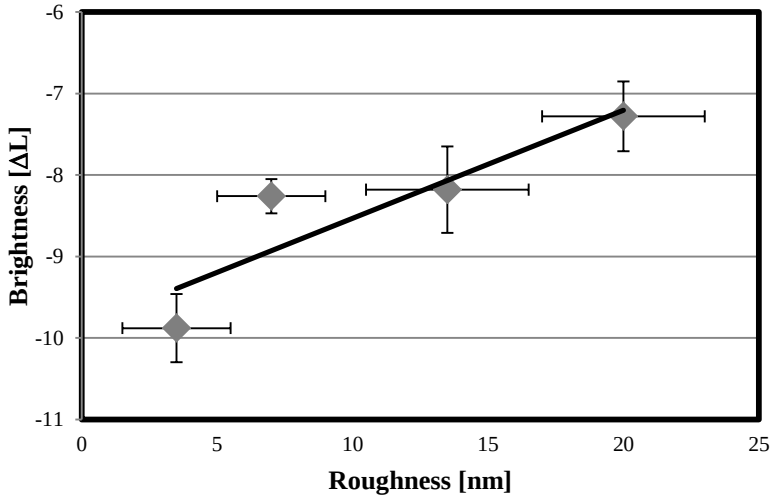

Fig. 1. Relationship between the roughness (nm) of the coated Typha fibers measured with the AFM (Atomic force microscope) and the brightness difference in the coated oak wood (measured before and after the oil treatment)

The reason for this effect seems to be the relatively stronger diffuse reflection associated with an increased nanometer-scale roughness. Parts of the incoming light reflect specularly on a smoother surface, but not all of it does. A portion of the incident light gets reflected diffusely to a varying degree. The greater the dispersion of light is, the brighter the sample appears. This effect can also be found in several other studies (Klein 2004; Meichsner *et al.* 2011). For example, rougher pigments appear much brighter than

smooth pigments (Klein 2004). The correlation of nanoroughness with brightness (Fig. 1) is non-trivial, as the roughness is well below the visible wavelength. Although the nano-roughness is below the wavelength of light, minor local surface irregularities may still lead to diffused light reflections.

Non-homogeneities in the distribution of the oils or different interactions with the wood can be alternatively explained by a similar physical effect. Thereby, to varying degrees, diffuse light from the entire reflected radiation will be filtered. This means that thicker layers and more homogeneous coatings filter more diffuse light due to back reflection; consequently, the surface appears darker (Meichsner *et al*. 2011). The differences between the homogeneous and smooth linseed oil and the rather rough and inhomogeneous sunflower oil can be seen in Fig. 2.

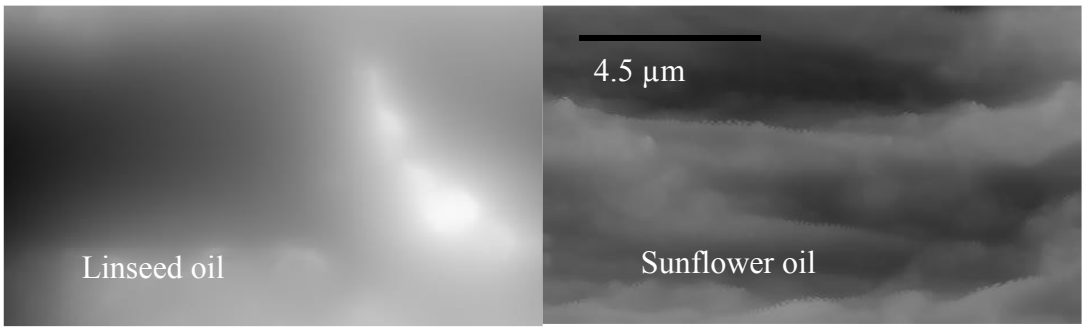

Fig. 2. Two AFM images (topography images) of linseed oil- and sunflower oil-coated Typha fibers

However, with the data available at present, it is very difficult to determine which of these effects is crucial for the altered appearance of wood. Therefore, a second method was used to change the roughness of the wood in the nanometer range without applying any substance. Due to UV-irradiation, the nanoroughness of the wood was altered. With a longer exposure to UV radiation, the roughness of the measured surface decreased (Fig. 3[a]). This effect was also detected in the work of Meincken and Evans (2009), in which the samples were exposed to sunlight. From an initial peak, the roughness subsequently decreased to a minimum level, only to increase again after a long exposure time. In the present work, not only has the nanoroughness changed due to the UV-irradiation, but there was also a change in color (Fig. 3[b]).

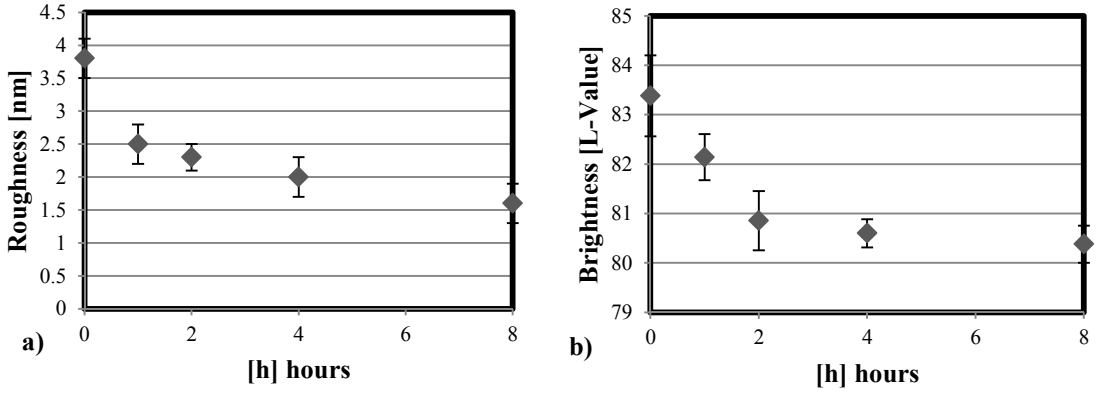

Fig. 3. The measured roughness [a] and brightness [b] after each UV-irradiation step

The maple thin sections got darker after every step of the UV-irradiation. Similar to the oil-coated samples, a significant amount of variability in brightness could be explained by the measured nanoroughness ($R^2 = 0.90$).

To analyze chemical changes due to the UV-irradiation, FTIR-ATR measurements were carried out. The measured spectra from FTIR-ATR showed minor changes; after eight hours of UV-irradiation, a clear increase in carbonyl groups (1734 cm^{-1}) and a decrease at the aromatic lignin C=C band (1505 cm^{-1}) was found (Fig. 4).

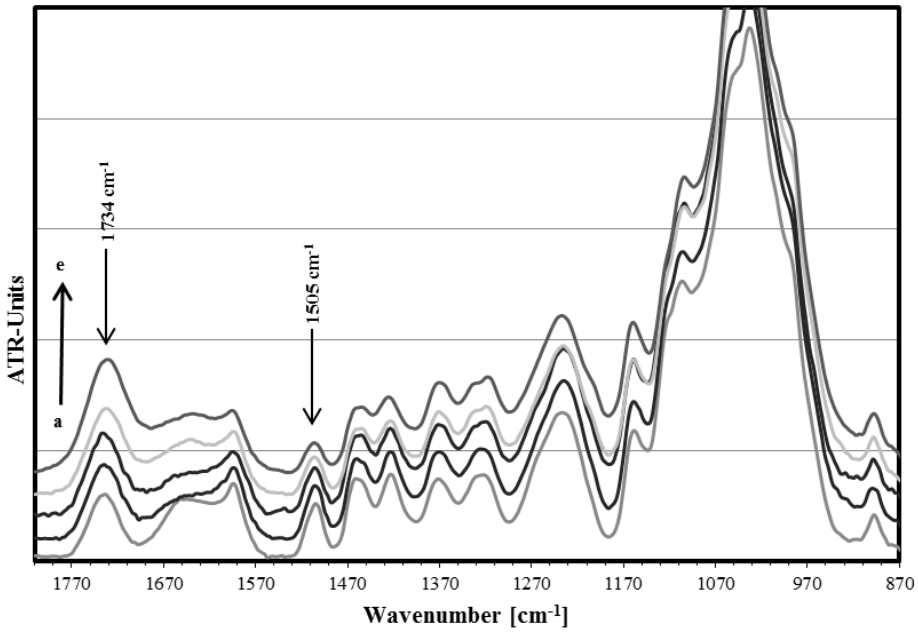

Fig. 4. Vector normalized (at 1375 cm^{-1}) FTIR spectra of maple wood irradiated for (a) 0 h, (b) 1 h, (c) 2 h, (d) 4 h, and (e) 8 h.

Furthermore, it can be seen that the ratio between the carbonyl and carbohydrates (Fig. 5[a]) and the ratio between the lignin and carbohydrates (Fig. 5[b]) both correlated with the brightness of the measured maple thin sections.

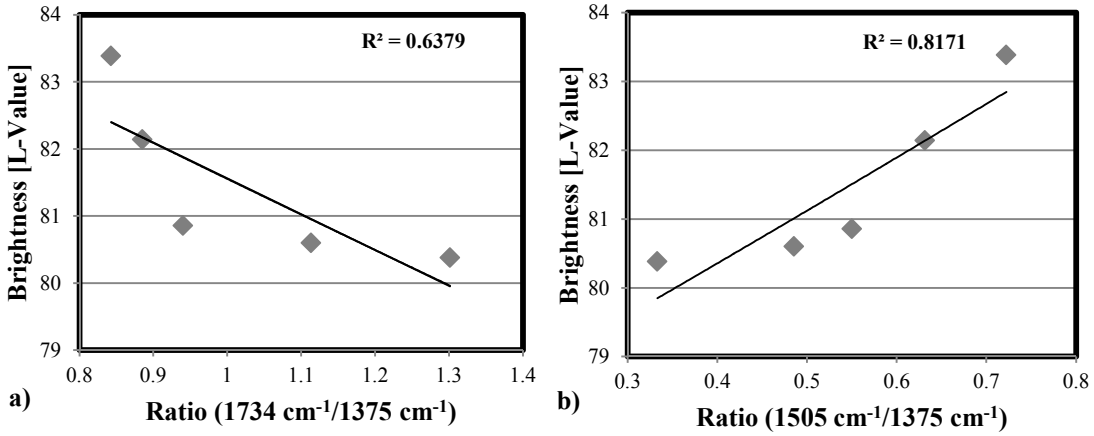

Fig. 5. Correlation of the brightness change (L-Value) and the increase in carboxyl groups [a] as well as the decrease in lignin [b]

In the literature, only strong chemical alterations wherein a degradation of lignin can be clearly seen have been associated with changes in color (Pandey 2005). Due to the measured spectra, chemical changes must be considered to explain the color changes. Both the measured chemical and structural changes correlate with the brightness of the prepared sample. This shows that both have an effect on the resulting appearance of wood. Because it is very difficult to change the nano-scale surface structure of wood without changing the surface chemistry, a quantification of the structural effects remains challenging.

The experiments presented show that the influence of the surface structure could be a partial factor for the appearance of wood. The identified correlations and the evidence from the literature should be reason for further investigation. However, a new approach should be found to characterize the influence of the surface structure. Further studies on this issue should clarify the influence of these effects on the general appearance of wood, independent of the processing or treatment.

CONCLUSIONS

1. This investigation has been carried out to test the surface roughness of wood and its influence on the appearance. The results show that a clear correlation exists between the nanoroughness, which was altered by oil coatings and UV irradiation, and the brightness of the wood surface. This indicates a hitherto unconsidered effect of the surface roughness on the appearance of wood.
2. Due to a similar trend found for surface chemistry changes, no quantification of the strength of this effect can be given at this point.

ACKNOWLEDGMENTS

The authors wish to thank the Team7 Company for the funding and support of this project.

REFERENCES CITED

De la Rie, R. E. (1987). "The influence of varnishes on the appearance of paintings," *Studies in Conservation* 32(1)1-13.

DIN 6174 (1979). *Colorimetric Evaluation of Colour Differences of Surface Colours According to the CIELAB Formula.*

Gierlinger, N., Jacques, D., Grabner, M., Wimmer, R., Schwanninger, M., Rozenberg, P., and Pâques, L. E. (2004). "Colour of larch heartwood and relationships to extractives and brown-rot decay resistance," *Trees - Structure and Function* 18(1), 102-108.

Gindl, W., Gupta, H. S., and Grünwald C. (2002). "Lignification of spruce tracheid secondary cell walls related to longitudinal hardness and modulus of elasticity using nano-indentation," *Canadian Journal of Botany* 80(10), 1029-1033.

ISO 4892-2 (2013). *Plastics - Methods of Exposure to Laboratory Light Sources - Part 2: Xenon-arc Lamps*, International Organization for Standardization.

Klein, G. A. (2004). *Farbenphysik für Industrielle Anwendungen*, Springer-Verlag, Heidelberg.

Koljonen, K., Österberg, M., Johansson, L. S., and Stenius, P. (2003). "Surface chemistry and morphology of different mechanical pulps determined by ESCA and AFM," *Colloids and Surfaces A: Physicochemical and Engineering Aspects* 228(1-3), 143-158.

Meichsner, G., Hiesgen, R., Esslinger, A., and Schottka, A. (2011). "Richtig anfeuern: Farbmetrische Charakterisierung von Holzoberflächen," *Farbe und Lacke* 117(12), 24-29.

Meincken, M., and Evans, P. (2009). "Nanoscale characterization of wood photodegradation using atomic force microscopy," *European Journal of Wood and Wood Products* 67(2), 229-231.

Moya, R., Fallas, R. S., Bonilla, P. J., and Tenorio, C. (2012). "Relationship between wood color parameters measured by the CIELab system and extractive and phenol content in *Acacia mangium* and *Vochysia guatemalensis* from fast-growth plantations," *Molecules* 17(4), 3639-3652.

Norrstrom, H. (1969). "The colour of unbleached sulphate pulp," Svenska Träforskningsinstitutet, Stockholm.

Pandey, K. K. (2005). "Study of the effect of photo-irradiation on the surface chemistry of wood," *Polymer Degradation and Stability* 90(1), 9-20.

Tshabalala, M. A., Kingshott, P., VanLandingham, M. R., and Plackett, D. (2003). "Surface chemistry and moisture sorption properties of wood coated with multifunctional alkoxysilanes by sol-gel process," *Journal of Applied Polymer Science* 88(12), 2828-2841.

Vorreiter, L. (1949). *Holztechnologisches Handbuch Band 1*, Verlag Georg Fromme & Co, Wien.

Watanabe, S., Sato, H., Shibuichi, S., Okamoto, M., Inoue, S., and Satoh, N. (2007). "Formation of nanostructure on hair surface: Its characteristic optical properties and application to hair care products," *Journal of Cosmetic Science* 58(4), 283-294.

Article submitted: April 22, 2013; Peer review completed: May 27, 2013; Revised version received and accepted: June 6, 2013; Published: June 11, 2013.

Paper 4 - Variability in Surface Polarity of Wood by Means of AFM Adhesion Force Mapping

Colloids and Surfaces A: Physicochem. Eng. Aspects 457 (2014) 82–87

Contents lists available at ScienceDirect

Colloids and Surfaces A: Physicochemical and Engineering Aspects

journal homepage: www.elsevier.com/locate/colsurfa

Variability in surface polarity of wood by means of AFM adhesion force mapping

Stephan Frybort[a,*], Michael Obersriebnig[b], Ulrich Müller[b], Wolfgang Gindl-Altmutter[b], Johannes Konnerth[b]

[a] Kompetenzzentrum Holz GmbH, Linz, Austria
[b] Institute of Wood Technology and Renewable Materials, Department of Material Sciences and Process Engineering, BOKU-University of Renewable Resources and Life Science, Vienna, Austria

HIGHLIGHTS

- Polarity of wood surfaces was measured by means of AFM adhesion force mapping.
- Microstructural variability in polarity of wood can be imaged by AFM at atmospheric conditions.
- Differences in polarity of freshly cut and native surfaces correlate with chemical heterogeneity.
- Surface ageing of wood originates almost exclusively from changes in freshly cut secondary cell walls S2.
- Native inner lumen surfaces hardly contribute to surface ageing.

GRAPHICAL ABSTRACT

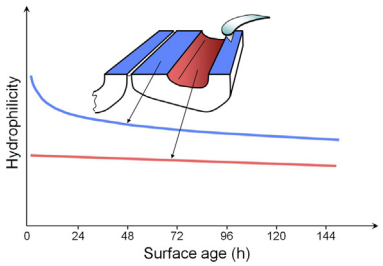

ARTICLE INFO

Article history:
Received 19 March 2014
Received in revised form 21 May 2014
Accepted 22 May 2014
Available online 2 June 2014

Keywords:
AFM
Adhesion force
Surface inactivation
Wood

ABSTRACT

The adhesion force between polar AFM tips and freshly cut wood surfaces was studied using AFM adhesion force mapping. Clear differences in polarity were found at microstructural level between freshly cut cell walls and native inner cell surfaces. Distinctly higher polarity in freshly cut cell walls is attributed to an abundance of accessible hydrophilic carbohydrate cell wall polymers compared to native cell surfaces. In good agreement with macroscopic studies of wood surface inactivation, the polarity of freshly cut cell walls showed a significant decrease with increasing surface age. Since such a decrease was observed to a much lesser degree in native inner surfaces compared to freshly cut cells it is proposed that predominantly the inactivation of freshly cut cell walls is responsible for overall surface inactivation phenomena in wood. It is concluded that the wood surface is heterogeneous in polarity, and that only the primarily hydrophilic wood surface regions are subject to inactivation, whereas surface chemistry of inner cell wall surfaces is very little affected by surface age.

1. Introduction

Wood is the most abundant natural material. As a bio-based and renewable resource it is of high importance for the building and furniture industry. In the assembly of modern wood-based composites, adhesive bonding is a crucial step. Variability in surface energy is a key factor in adhesion, because it determines

* Corresponding author. Tel.: +43 1 47654 4298; fax: +43 1 47654 4295.
E-mail addresses: s.frybort@wood-kplus.at, s.frybort@kplus-wood.at (S. Frybort).

http://dx.doi.org/10.1016/j.colsurfa.2014.05.055
0927-7757/

hydrophilicity, which is prerequisite for wetting of the wood surface by the majority of presently used wood adhesives [1]. Wood surfaces can be described as soft, porous, uneven, density varying, self-contaminating, predominantly hydrophilic, hygroscopic, and anisotropic [2,3]. Due to their self-contaminating and hygroscopic nature freshly cut wood surfaces are vulnerable to inactivation processes. Inactivation causes a reduction of surface polarity resulting in decreased surface wettability with polar liquids [4]. Thus it directly affects bonding quality of aqueous and other polar-based adhesives in a potentially negative manner. In order to prevent this, adhesive bonding of wood has to be carried out within no more than 24 h after machining of the new surface by e.g. planning or sawing. In case of highly resinous species, only a maximum of 6 h of time elapsed is tolerated [5].

Variability in wettability of a surface is largely determined by surface chemistry, besides other factors such as e.g. surface roughness. The polar character of a wood surface arises from accessible hydroxyl groups in the cell wall polymers and may also vary with the amount and composition of extractives. This implies that higher amounts of highly polar cellulose or hemicellulose accessible on a wood surface lead to a higher hydrophilicity compared to surfaces rich in lignin, which is less polar [6]. It is assumed, that the main drivers for inactivation are water and to a lesser extent low-molecular-weight volatile organic compounds [3], airborne contaminations [7], oxidation processes [8], and self-contamination by low-molecular wood extractives migrating to the wood surface [9]. These substances are able to form a layer on the surface leading to a decreased polarity, which in turn reduces wettability of the lignocellulosic substrate by aqueous liquids. Measurement of the contact angle of a sessile liquid drop deposited on a surface is an established method for the assessment of wettability of a solid surface [10,11]. Contact angle measurements on wood surfaces are affected by variables such as surface roughness [12], temperature [13], chemical heterogeneities [14] and wood moisture content [15]. Most importantly, owing to the significant drop volume of several μl required (2–6 μl according to DIN EN 828 [16]) this method only delivers macroscopic information. This is a severe limitation when one considers the fact that a typical wood surface produced by machining consists on the one hand of freshly cut cell walls, and on the other hand of native inner cell surfaces on the inner sides of cell cavities (lumen), and is thus distinctly heterogeneous at micron scale. The present study aims to investigate potential heterogeneity in wettability associated with variability in the morphology of the wood surface. Since such variability is most probably averaged out in contact angle measurement, a method capable of higher spatial resolution is required.

Atomic force microscopy (AFM) resolves surface features down to nanometer spatial resolution and is therefore a powerful tool for the examination of the micro- and nanostructure of the wood cell wall. AFM is widely used for imaging as well as for mechanical and chemical characterization of different fiber materials [17–19] and for wood surfaces [20,21]. Atomic force spectroscopy is an operating mode of AFM which allows quantifying adhesion between probe and surface [22]. In such an experiment, intermolecular forces are obtained from the force–distance curve which is recorded for every measured pixel [23]. Compared to other techniques AFM adhesion force measurement is largely unaffected by macroscopic chemical inhomogeneity and surface roughness, and it is surface specific [24]. It has already been shown that AFM is capable of determining microstructural variability in the surface polarity of wood surface [21]. Building on this experience, we aim to detect potential time dependent changes of the polarity and thus hydrophilicity in different microstructural regions of wood surfaces.

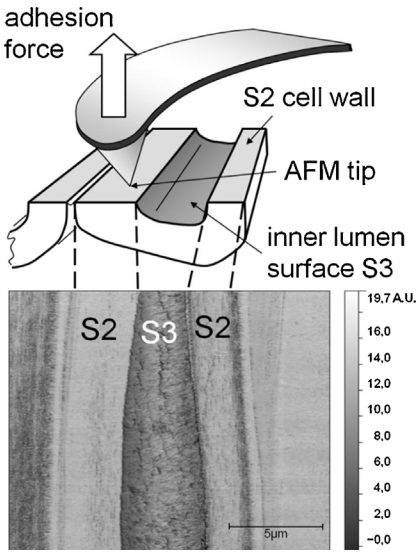

Fig. 1. Top: schematic diagram of the cell-wall surfaces characterized: the S2 cell wall layer is freshly cut during the machining process while the inner surface of the cell cavity (lumen) termed S3 is a native inner surface. Bottom: adhesion map of the specimen showing variable adhesion values depending on the type of cell-wall measured: freshly cut secondary cell walls (S2) show high adhesion compared to native inner lumen surfaces (S3).

2. Materials and methods

2.1. Sample preparation

For acclimatization wood samples with gross dimensions of $10 \times 10 \times 10\,mm^3$ were stored inside the AFM measuring room for about one week at controlled conditions of 23 °C and 50% relative humidity. In order to decrease necessary cutting forces and thus mechanical impact on the surface for the subsequent ultramicrotoming process step wood tangential surfaces were reduced conically to approx. $1.5 \times 3\,mm^2$. To provide smooth latewood surfaces the reduced tangential surfaces of the specimens of both spruce wood (*Picea abies* Karst.) and beech wood (*Fagus silvatica* L.) were finally cut using a histo diamond knife mounted on an ultramicrotome (Ultracut R, Leica, Germany) by removing sections down to a thickness of 50 nm. Special care was taken not to contaminate the surface in any step. Immediately after surface preparation the specimen was mounted to the AFM stage and measurements started at the latest within 2 h after sample preparation. The examined regions of the wood surface in terms of cell walls and orientation of the exposed section in relation to the wood anatomical directions are exemplarily shown in Fig. 1.

2.2. Atomic force microscopy

In the wood species investigated, the potential maximum variations in height between lumen (S3) and freshly cut secondary cell wall (S2) areas correspond to the diameter of the lumen, which is typically ≤20 μm. Since imaging of a surface with such a high roughness exceeds the capability of the set-up chosen in the present study, with a tip length of 5 μm of the AFM probe, less rough imaging locations toward the ends of cut-open fiber cells were identified by light microscopy prior to AFM. AFM-topography imaging was performed with a Dimension Icon Scanning Probe Microscope (Bruker AXS, France; formerly Veeco) equipped with a NanoScope V control station. Adhesion force mapping was carried out using an untreated silicon tip mounted on a silicon nitride cantilever (Scanasyst-Air, Bruker, USA; cantilever stiffness 0.5 N/m) in Peak Force Quantitative Nanomechanical Mapping Mode (Peak Force

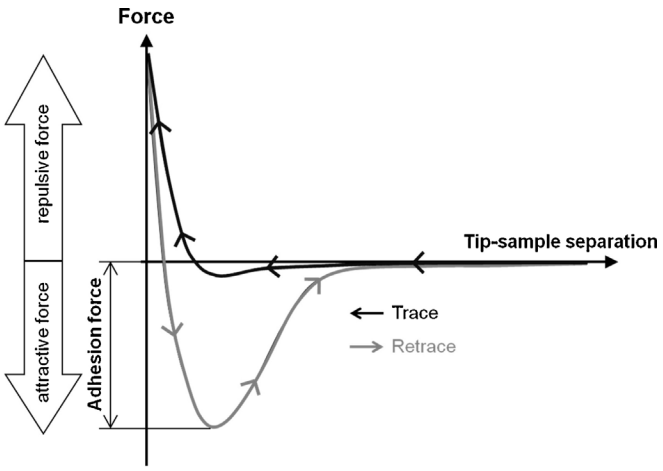

Fig. 2. Exemplary force distance curve from adhesion force mapping measurement. Adhesion force is obtained from the peak force measured during the retrace (unloading) cycle.

QNM®, Bruker). In QNM the loading and unloading force–distance curves are collected at a frequency of either 1 or 2 kHz at each position within the mapped area of the specimen. In parallel to topography, information on material elasticity and tip-to-surface adhesion force is obtained and displayed in the respective pixel of an AFM image [25].

A schematic force–distance curve is shown in Fig. 2. While no force is observed at large distance, attractive forces act at smaller distance until contact is established and the tip is eventually pushed into the surface until a pre-defined set-point. The cantilever is then retracted while the tip maintains surface contact until the spring force of the cantilever overcomes adhesion forces leading to a separation of the probe [26]. The maximum force for detaching the tip from the surface corresponds to the adhesion forces between the surface and the tip of the probe [22]. The tip used in the present study shows distinctly higher adhesion forces to polar surfaces compared to unpolar surfaces [21] and is thus representative of attraction of polar molecules between surface and tip. Since the pull-off force is proportional to the local adhesion energy [6], measured adhesion forces provide relative information about the degree of hydrophilicity of the surface [27].

Specimens were repeatedly characterized during a period starting within 2 h after surface preparation until 144 h after the new surface was created. In order to avoid dimensional changes these long term measurements were performed under controlled constant climate conditions (23 °C, 50% RH). Also, machine drift was reduced to a minimum by activating the AFM hardware at least one day before the start of the first measurement. The cantilever stiffness was measured for each cantilever used by thermal tuning and was in the range of 0.5 N/m. The deflection sensitivity of the cantilever was measured by acquiring a force–distance curve on a sapphire reference surface. The nominal tip radius of 5 nm indicated by the manufacturer was used for all evaluations, since primarily relative comparisons within individual images acquired were of interest. Force–distance measurements as indicated exemplarily in Fig. 2 were carried out with a peak force amplitude of 150 nm and a scan rate of 0.3 Hz. A small peak force amplitude (set-point) minimizes tip wear [28], which is mandatory for the long-term measurements performed. Long-term measurements by AFM are restricted to the life-span of the probe. For the present wood specimens after about 40 scans the wear of the tip of the probe leads to artifacts which got visible in asymmetric adhesion maps, especially of the normally symmetric adhesion forces within the native inner lumen surface (S3).

Fig. 3 gives an overview of the examined regions of the two wood species in the present study. Fig. 3a shows a tracheid of spruce. The vertical part in the middle of the figure represents the uncut secondary cell wall 3 (S3) of the lumen which is flanked by the freshly cut open secondary cell wall 2 (S2). Fig. 3b shows a fiber of beech, again the vertical part in the middle of the figure represents the lumen of the fiber with its characteristic warty structure. The lower region of the lumen shows an artifact which was caused by sample preparation. In this region the S3 was torn off exposing the underlying S2. For this case analysis of adhesion force was limited to the upper part of the lumen with its characteristic warty structure.

2.3. Evaluation of AFM measurements

Adhesion force maps are displayed in Fig. 4, where light grey represents high adhesion force and dark grey low adhesion force, respectively, between probe tip and wood surface. For the calculation of the average adhesion forces of the individual cell regions the values of the corresponding S2 and S3 region (Fig. 4, regions labeled with color) were acquired, areas of interest e.g. freshly cut cell walls

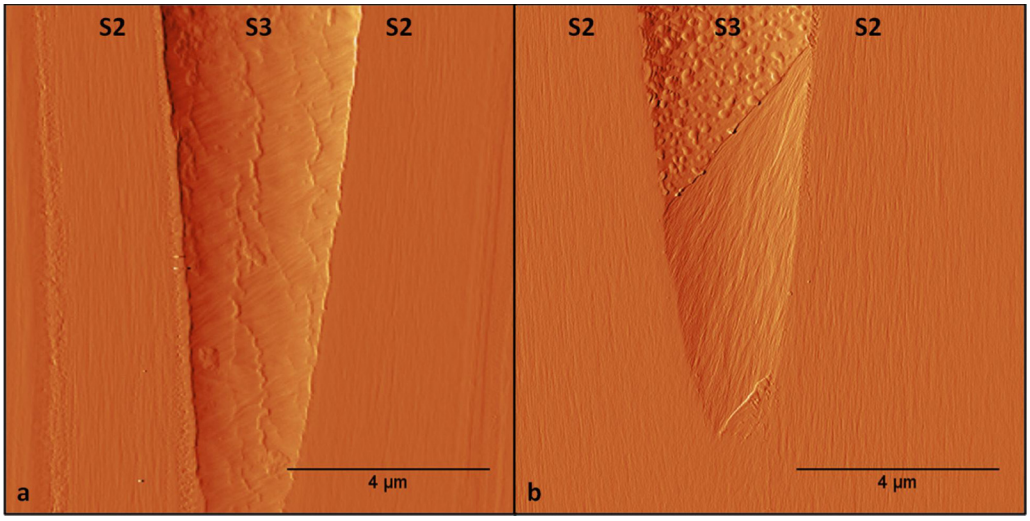

Fig. 3. Peak force error maps of representative areas of cut wood surfaces selected for examination with quantitative nanomechanical mapping. (a) Spruce, (b) beech. (S2) Freshly cut cell walls, (S3) native inner lumen surface easily discernible by its comparably higher roughness.

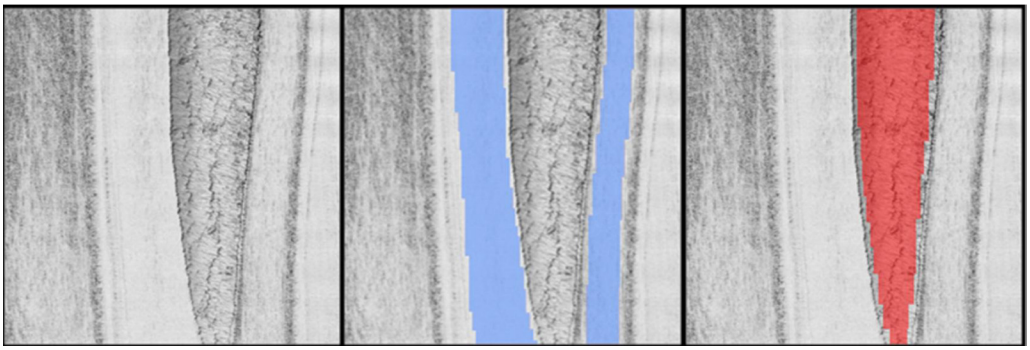

Fig. 4. Left: representative adhesion force map measured for spruce wood (light regions of the image indicate high adhesion force whereas darker regions correspond to lower adhesion force). Centre (blue): freshly cut cell wall region (S2) selected for averaging of adhesion force values. Right (red): native inner lumen surface (S3) selected for averaging. Average values obtained were used for further analysis. (For interpretation of the references to color in this figure legend, the reader is referred to the web version of this article.)

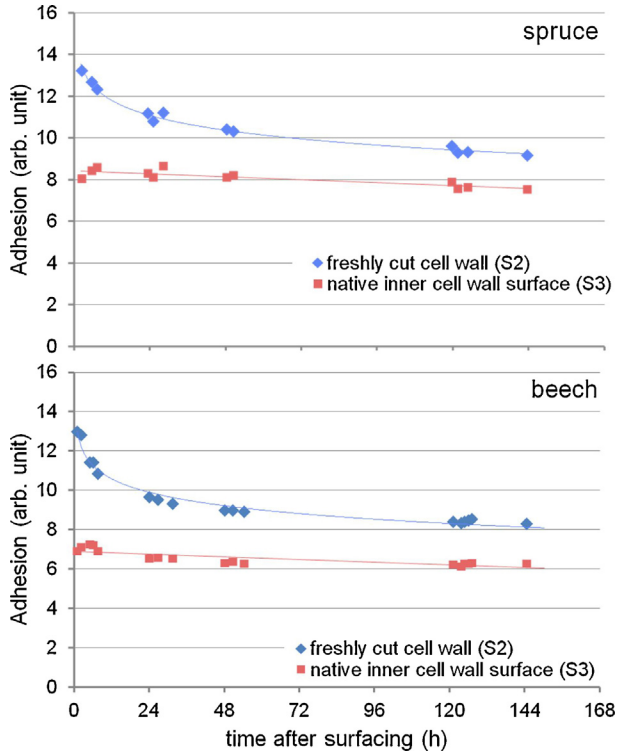

Fig. 5. Variability of AFM adhesion force in freshly cut cell walls (S2) compared to native inner lumen surfaces (S3) with increase of time elapsed between surface generation by machining and characterization. Each pair of S2/S3 data points represents the average of one recorded adhesion force map.

were selected, marked, and analyzed using the open source software Gwyddion 2.29. Mean values of the adhesion for the individual areas of the two wood species were plotted against time in Fig. 5.

3. Results

A representative example of the morphological regions of cut wood surfaces examined in the present study is given in Fig. 3. In both wood species studied, regions with limited height difference between freshly cut secondary cell walls (S2) and native inner lumen surfaces (S3) were selected in order to enable imaging in the AFM. Visual inspection of the specimen surfaces shown in Fig. 3 reveals very low roughness in freshly cut cell walls, whereas the native inner surface of the lumen exhibits distinct surface roughness. Adhesion force maps acquired for such sample areas were evaluated semi-quantitatively by calculating average values of adhesion force for selected areas within the adhesion force map as shown in Fig. 4. Thus, two data points each, one corresponding to S2 and one corresponding to S3, were extracted for each adhesion force map acquired and used for further analysis.

The results of this analysis, i.e. the variability of adhesion force in freshly cut cell walls (S2) compared to native inner lumen surfaces (S3) is shown in Fig. 5 for both wood species studied.

The sets of measurements acquired for spruce and beech wood, respectively, are very similar both on absolute terms and also with regard to the trend observed with increasing surface age. In general, clearly higher values of adhesion force were recorded for freshly cut cell walls (S2) compared to native inner lumen surfaces (S3). Also, S2 values show a very clear initial phase of rapidly decreasing adhesion force, which flattens out after approx. two days. A slight decrease is also apparent for S3 values, however, the decrease is much less pronounced than found in S2, and it follows a linear trend.

4. Discussion

4.1. Microstructural heterogeneity of adhesion force

The significant difference in adhesion force measured between freshly cut cell walls (S2) and native inner lumen surfaces (S3) indicates variability in surface chemistry of these two morphological regions (Fig. 5). Compared to the bulk S2 cell wall layer, the inner layer covering the S3 (warty layer) is proposed to be characterized by a higher degree of lignification [29,30]. Comparing surface energy of lignin and cellulose, Notley and Norgren [31] observed only minor differences in total free surface energy of these two most important wood cell wall polymers. However, the polar component of surface free energy [32] was significantly more pronounced in cellulose compared to lignin, leading to a better wettability of cellulose with water compared to lignin. This implies that higher amounts of cellulose accessible on the surface lead to a higher hydrophilicity whereas higher amounts of lignin lead to a reduction in hydrophilic character [6]. In line with this reasoning we propose that differences in adhesion force between different types of wood surface measured in the present study are caused by concurrent differences in surface polarity. The interpretation of variable adhesion force in terms of changes in polarity, and further on hydrophilicity is confirmed by micromechanical findings comparing adhesion of urea-formaldehyde wood adhesive to the two respective morphological regions studied here [21]. In nanoindentation-based direct measurements at the immediate adhesive to wood interface the adhesion of cured urea-formaldehyde to freshly cut cell walls presumed more hydrophilic than inner lumen surfaces was

significantly stronger (+60%) than interaction with the latter surface presumed less hydrophilic.

Interpretation of the adhesion force measured by AFM is complex as complications may arise due to atmospheric humidity. At atmospheric conditions, adhesion forces measured are a combination of attractive van der Waals forces between probe and surface, which are the actual subject of interest, and water surface tension due to capillary condensation between tip and surface [23]. However, in practice this phenomenon is not problematic within the frame of the present study, because, when studying variability in hydrophilicity, also the build-up of a capillary water bridge due to meniscus formation between tip and sample surface provides information about the hydrophilicity of the surface [27]. A conventional method to prevent meniscus formation is measuring in liquid [24] or absolute dry environment (vacuum). However, wood experiences an alteration in its surface-chemical and mechanical properties when in contact with liquid as well as when dried, which is why this option was discarded. This decision is supported by the fact that a suitable relative humidity can even enhance image contrast in adhesion to surfaces of varying polarity. Chen et al. [33] showed that contrast between polar and less polar surfaces is highest at 45 to 70% relative humidity. This observation is believed to be related to the fact that a surface of high polarity is characterized by a higher density of adsorbed water molecules than a surface of comparably lower polarity. In this context, the measurement conditions of 23 °C and 50% relative humidity seem favorable. The presence of capillary water bridges becomes noticeable when a sudden "jump to contact" is recorded as the probe approaches the surface. In this case the same jump is again observed within the retrace curve when detaching the probe from the surface. These phenomena occur when capillary bridges form and break between sample surface and probe, respectively [6,27]. In the present study neither of these phenomena was observed.

To conclude this section, it is proposed that the differences in adhesion force measured for the two morphological regions in wood surfaces are correlated with differences in surface chemistry, presumably the ratio of lignin to cell wall carbohydrates, and that there is no negative effect of humidity on the results measured.

4.2. Variability of adhesion force with surface age

In addition to significant overall differences in measured adhesion force between freshly cut cell walls and native inner lumen surfaces, the pattern of change in adhesion force with increasing surface age is also clearly different. Native inner lumen surfaces only show a very slight decrease in adhesion force during the period of six days within which measurements were carried out. This effect could possibly be attributed to a certain drift of measurements with time or by further changes of the newly opened surface whereby molecules from the surrounding atmosphere are able to contaminate the surface. In contrast, freshly cut cell walls exhibit a strong decrease in adhesion force within the first 24 h after cutting. Thereafter, a trend of further decrease at lower rate follows. The pattern of surface inactivation exhibited by freshly cut cell walls is in excellent agreement with macroscopic observations of surface activation in wood using contact angle measurements [4]. We therefore propose that surface inactivation phenomena in planed, sawn, or otherwise machined wood surfaces originate from changes in the surfaces of freshly cut cell walls, whereas native inner lumen surfaces exposed by machining only slightly contribute to such changes. Even though the polar component of surface energy amounts only to about 20% of the total surface free energy of wood [34], it is critical to the wetting of wood with water or aqueous systems in general. Consequently, contact angle measurement revealed mainly a decrease in the polar component of surface energy with increasing surface age, whereas the dispersive component showed only little change [4]. Again there is a good agreement between the macroscopic observation by contact angle measurement, and AFM adhesion force mapping, as both methods reveal decreasing surface polarity.

5. Conclusion

In conclusion, the present study contributes significant new aspects to the understanding of wood surface chemistry. It was demonstrated that:

- microstructural variability in polarity of wood surfaces can be imaged by means of AFM using regular silicon AFM tips at atmospheric conditions,
- differences in polarity between freshly cut cell walls and native inner lumen surfaces correlate with chemical heterogeneity, in particular varying ratio of lignin compared to cell wall carbohydrates, and
- surface ageing of wood originates almost exclusively from changes in freshly cut cell walls, whereas native inner lumen surfaces hardly contribute to this phenomenon.

Acknowledgments

Funding by Europäische Union/Europäischer Fonds für regionale Entwicklung (EFRE), Land Niederösterreich, Abteilung Wirtschaft, Tourismus und Technologie (Project No. WST3-T/022-2012), and the Austrian Science Fund FWF: Project No. P21681 is gratefully acknowledged.

References

[1] M. Dunky, P. Niemz, Holzwerkstoffe und Leime: Technologie und Einflussfaktoren, Springer Verlag, Berlin, Heidelberg, New York, 2002.
[2] R.M. Nussbaum, Natural surface inactivation of Scots pine and Norway spruce evaluated by contact angle measurements, Holz Roh—Werkst. 57 (1999) 419–424.
[3] C. Piao, J.E. Winandy, T.F. Shupe, From hydrophilicity to hydrophobicity: a critical review: Part I. Wettability and surface behavior, Wood Fiber Sci. 42 (2010) 490–510.
[4] M. Gindl, A. Reiterer, G. Sinn, S. Stanzl-Tschegg, Effects of surface ageing on wettability, surface chemistry, and adhesion of wood, Holz Roh Werkst. **62** (2004) 273–280.
[5] ÖNORM, Brettschichtholz—Leistungsanforderungen und Mindestanforderungen an die Herstellung, in: ÖNORM EN 386, ÖNORM, 2002.
[6] F.L. Leite, P.S.P. Herrmann, A.L. Da Róz, F.C. Ferreira, A.A.S. Curvelo, L.H.C. Mattoso, Investigation of sisal fibers by atomic force microscopy: morphological and adhesive characteristics, J. Nanosci. Nanotechnol. 6 (2006) 2354–2361.
[7] I. Aydin, Activation of wood surfaces for glue bonds by mechanical pretreatment and its effects on some properties of veneer surfaces and plywood panels, Appl. Surf. Sci. 233 (2004) 268–274.
[8] S.-Z. Chow, Infrared spectral characteristics and surface inactivation of wood at high temperatures, Wood Sci. Technol. 5 (1971) 27–39.
[9] E.L. Back, Oxidative activation of wood surfaces for glue bonding, For. Prod. J. 41 (1991) 30–36.
[10] P.F. Liu, D.J. Gardner, M.P. Walcott, A model for the description of polymer surface dynamic behaviour. Contact angle vs polymer surface properties, Langmuir 11 (1995) 2674–2681.
[11] G.I. Mantanis, R.A. Young, Wetting of wood, Wood Sci. Technol. 31 (1997) 339–353.
[12] D.A. Doshi, P.B. Shah, S. Singh, E.D. Branson, A.P. Malanoski, E.B. Watkins, J. Majewski, F. van Swol, C.J. Brinker, Investigating the interface of superhydrophobic surfaces in contact with water, Langmuir 21 (2005) 7805–7811.
[13] D.W. Gunnels, D.J. Gardner, M.P. Wollcott, Temperature dependence of wood surface free energy, Wood Fiber Sci. 26 (1994) 445–447.
[14] A. Marmur, Equilibrium contact angles: theory and measurement, Colloids Surf., A: Physicochem. Eng. Aspects 116 (1996) 55–61.
[15] M. Scheikl, M. Dunky, Measurements of dynamic and static contact angles on wood for the determination of its surface tension and the penetration of liquids into the wood surface, Holzforschung 52 (1998) 89–94.
[16] DIN, Klebstoffe—Benetzbarkeit—Bestimmung durch Messung des Kontaktwinkels und der freien Oberflächenenergie fester Oberflächen, in: DIN EN 828, DIN, 2013.

[17] J.C. Bastidas, R. Venditti, J. Pawlak, R. Gilbert, S. Zauscher, J.F. Kadla, Chemical force microscopy of cellulosic fibers, Carbohydr. Polym. 62 (2005) 369–378.
[18] G. Raj, E. Balnois, C. Baley, Y. Grohens, Adhesion force mapping of raw and treated flax fibres using AFM force-volume, J. Scanning Probe Microsc. 4 (2009) 66–72.
[19] A. Klash, E. Ncube, M. Meincken, Localization and attempted quantification of various functional groups on pulpwood fibres, Appl. Surf. Sci. 255 (2009) 6318–6324.
[20] M. Meincken, P.D. Evans, Nanoscale characterisation of wood photodegradation using atomic force microscopy, Eur. J. Wood Wood Prod. 67 (2009) 229–231.
[21] M. Obersriebnig, J. Konnerth, W. Gindl-Altmutter, Evaluating fundamental position-dependent differences in wood cell wall adhesion using nanoindentation, Int. J. Adhes. Adhes. 40 (2013) 129–134.
[22] A. Noy, D.V. Vezenov, C.M. Lieber, Chemical force microscopy, Annu. Rev. Mater. Sci. 27 (1997) 381–421.
[23] B. Cappella, G. Dietler, Force–distance curves by atomic force microscopy, Surf. Sci. Rep. 34 (1999) 1–104.
[24] A. Pietak, S. Korte, E. Tan, A. Downard, M.P. Staiger, Atomic force microscopy characterization of the surface wettability of natural fibres, Appl. Surf. Sci. 253 (2007) 3627–3635.
[25] W.F. Heinz, E. A-Hassn, J.H. Hoh, Application of force volume imaging with atomic force microscopes, in: Veeco Application Note AN20, Rev. A1, Veeco, 2004.
[26] F.L. Leite, P.S.P. Herrmann, Application of atomic force spectroscopy (AFS) to studies of adhesion phenomena: a review, J. Adhes. Sci. Technol. 19 (2005) 365–405.
[27] L. Sirghi, M. Nakamura, Y. Hatanaka, O. Takai, Atomic force microscopy study of the hydrophilicity of TiO_2 thin films obtained by radio frequency magnetron sputtering and plasma enhanced chemical vapor depositions, Langmuir 17 (2001) 8199–8203.
[28] A. Pakzad, J. Simonsen, R.S. Yassar, Gradient of nanomechanical properties in the interphase of cellulose nanocrystal composites, Compos. Sci. Technol. 72 (2012) 314–319.
[29] W.M. Bair, Development and Composition of the Warty Layer in Balsam Fir [Abies balsamea (L.) Mill.], Institute of Paper Chemistry, Lawrence University, Appleton, WI, 1974.
[30] W. Liese, Elektronenmikroskopie des Holzes, Umschau Verlag, Frankfurt, 1970.
[31] S.M. Notley, M. Norgren, Surface energy and wettability of spin-coated thin films of lignin isolated from wood, Langmuir 26 (2010) 5484–5490.
[32] R.J. Good, C.J. van Oss, The Modern Theory of Contact Angle and the Hydrogen Bond Components of Surface Energies, Marcel Dekker Inc., New York, NY, 1993.
[33] L. Chen, X. Gu, M.J. Fasolka, J.W. Martin, T. Nguyen, Effects of humidity and sample surface free energy on AFM probe—sample interactions and lateral force microscopy image contrast, Langmuir 25 (2009) 3494–3503.
[34] M. Gindl, Effects of Surface Free Energy on the Coating Properties of Wood, Institut für Holzforschung, Universität für Bodenkultur, Vienna, 2002.

Paper 5 - Studying Thermal Conductivity of Wood at Cell Wall Level by Scanning Thermal Microscopy (SThM)

Short Note

Oliver Vay, Michael Obersriebnig*, Ulrich Müller, Johannes Konnerth and Wolfgang Gindl-Altmutter

Studying thermal conductivity of wood at cell wall level by scanning thermal microscopy (SThM)

Abstract: Local variability in the thermal conductivity of the cell wall of beech wood fibers was studied by means of scanning thermal microscopy (SThM). In the cross section, the thermal conductivity of the secondary cell wall was essentially higher than that of the compound middle lamella (CML). In sections parallel to the cell axis, the overall conductivity of the S1 layer was lower than that of the secondary cell wall, but the S2 layer and the CML showed similar conductivities. This is attributed to the orientation of the cellulose microfibrils playing a key role in the observed anisotropies concerning the thermal conductivity. The deviating thermal conductivities on different sections are attributed to the depth effect of the thermal scanning. SThM proves to be a technique with considerable potential for wood research.

Keywords: scanning thermal microscopy (SThM), thermal conductivity, wood cell wall

***Corresponding author: Michael Obersriebnig,** BOKU, University of Natural Resources and Life Science, Department of Material Science and Process Technology, Vienna, Austria,
Phone: +43-1-47654-4290, Fax: +43-1-47654-4295,
e-mail: m.obersriebnig@boku.ac.at
Oliver Vay: Kompetenzzentrum Holz GmbH, Linz, Austria
Ulrich Müller: Kompetenzzentrum Holz GmbH, Linz, Austria
Johannes Konnerth: BOKU, University of Natural Resources and Life Science, Department of Material Science and Process Technology, Vienna, Austria
Wolfgang Gindl-Altmutter: BOKU, University of Natural Resources and Life Science, Department of Material Science and Process Technology, Vienna, Austria

Introduction

Anisotropy of structure and physical properties is a key characteristic of wood, which is extensively discussed in textbooks in terms of mechanics, swelling, and shrinkage, diffusion of moisture, and thermal conductivity along and transverse to the grain. The microstructural features of this property were reviewed recently by Hofstetter and Gamstedt (2009); see also Taguchi et al. (2011) and Bader et al. (2012). The structural and chemical reasons for anisotropy are also of high interest in wood science. New experimental techniques help to gain more insights with this regard. Nanoindentation (Wimmer et al. 1997; Follrich et al. 2010; Clauß et al. 2011; Lehringer et al. 2011; Yu et al. 2011) may serve as an example for such a new technique, which allows studying the properties of wood at the cell wall level. For example, the stiffness tensor components of the wood cell walls were inferred from such experiments (Jäger et al. 2011). Owing to its extremely versatile character and high resolution, scanning probe microscopy (SPM) is another method that is well capable of advanced studies of wood structure and structure-property relationships at the micro- and nanoscales. In addition to surface topography imaging (Fahlén and Salmén 2005), SPM tips with special functionalities permit physical characterization at the nanometer level with high resolution, leading to the data of surface chemistry (Bastidas et al. 2005) and micromechanics (Wagner et al. 2011). Scanning thermal microscopy (SThM), another specialized form of SPM, was used to study the distribution of adhesives in the wood cell wall by Konnerth et al. (2008), while Lee et al. (2009) applied this technique to visualize interfacial zones in lyocell fiber-reinforced PP composites. SThM detects the thermal properties of a sample with a resolution of tens of nanometers. To this purpose, a standard AFM probe is substituted with an electrically heated one. Better techniques replaced the original Wollaston wire probes with special contact mode probes, which incorporate a thin metal film near the apex of the probe as a conductive element and increased the resolution from about 1 µm to below 100 nm (Majumdar 1999; Shi et al. 2001). The new developments of SThM found widespread attention in material science, e.g., for failure analysis in the integrated circuits in the temperature contrast mode (Fiege et al. 1998) or for the analysis of composites (Blanco et al. 2002).

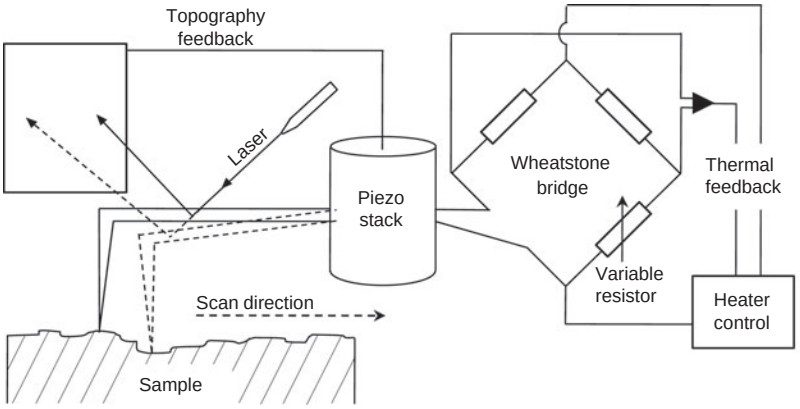

Figure 1 Schematic representation of the SThM setup. The SThM probe constitutes one of the resistors in a Wheatstone bridge, which allows gathering of thermal data via a feedback loop. The variable resistor is necessary to zero the output voltage prior to the measurements. At the same time, the standard AFM setup collects the topographic data of the surface.

The probe constitutes one of the resistors in a Wheatstone bridge (Figure 1). This allows monitoring the thermal changes in the probe via a feedback mechanism, while at the same time, topographical data are collected. Depending on the applied voltage, the probe can either act as a resistive thermometer for mapping the temperature distribution on the surface or as a resistive heater.

In the first case, the applied heating voltage is very low so that the probe temperature stays below the surface temperature. Bringing the tip in contact with the surface elevates the tip temperature, which changes the electrical resistance in the tip, and therefore, the output voltage can be measured between the branches of the Wheatstone bridge (temperature contrast mode).

In the second case, a relatively high voltage is applied, which elevates the tip temperature well above the sample temperature. Upon contact, the probe temperature diminishes as a function of the thermal conductivity of the sample. Via the feedback mechanism, the probe temperature is restored to its original value, while at the same time the thermal data are collected, thus providing a measure of thermal conductivity (conductivity contrast mode).

In the present paper, the conductivity contrast mode was selected to evaluate the thermal conductivity of the fibers at the cell wall level parallel and normal to the fiber axis. This type of experiment has not yet been described in the literature.

Materials and methods

Samples were small cubes of beech wood (*Fagus sylvatica*) smoothed with an ultramicrotome (Leica), with one sample prepared for every anatomical direction. Measurements were carried out on a Bruker Dimension Icon (Bruker, Santa Barbara, CA, USA) equipped with a standard SThM probe (VITA-DM-GLA 1, nominal tip radius <100 nm) of the same manufacturer. All measurements were performed with the same tip to prevent influences from varying tip radii, while applied pressure on the sample was kept low to minimize tip wear. The heating voltage of 2 V for all the scans provided good contrast. The scan size was 6 µm ×6 µm at a scan rate of 0.3 Hz with constant gain factors. To prevent drift artifacts in the thermal feedback cycle from the system electronics, a control measurement was performed at the beginning and end of each scan session. To this purpose, one position on the S2 cell wall layer of the cross section of a fiber was scanned. It showed that the drift during each session was negligible, if care was taken that the probe heating was only turned on directly before contacting the sample and turned off promptly after finishing the scan. The drift was significant only after long breaks (e.g., overnight); in such cases, a readjustment of the variable resistor was necessary. For comparability, a constant background was added or subtracted for all images, such that the average output voltage on the S2 layer at the control position of the respective scanning session was zero.

Results and discussion

In Figure 2a, the cross-section scan reveals a clear variation in the conductivity between the S2 layer and the compound middle lamella (CML), with lighter colors in the latter corresponding to a lower conductivity. Figure 2b and c are contrast images for topography and conductivity on a longitudinal section. Although the surface is overall rather flat, the vertical grooves are remarkable along the interface S1/CML and S1/S2, respectively. Being approximately the width of the tip, those grooves may lead to scanning artifacts in the thermal image due to an increase in the tip-sample contact area. Therefore, a seemingly increased conductivity, visible in Figure 2c, is observed. Apart from this artifact, the conductivity variations are rather low and less pronounced than on the cross-section image. The S2 layer and the CML show approximately the

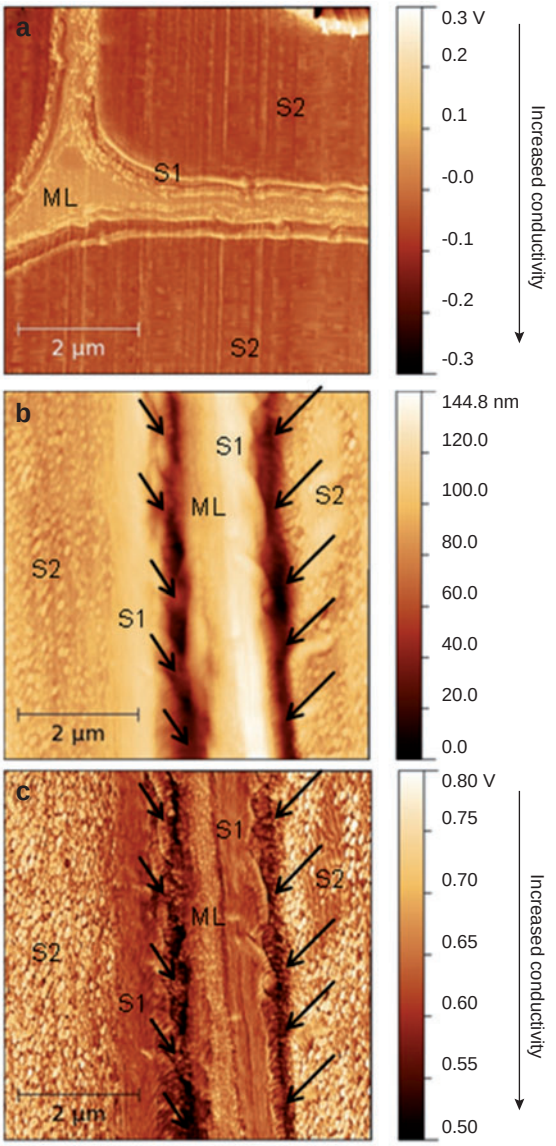

Figure 2 Representative scanning probe images from *Fagus sylvatica*. (a) Conductivity contrast image on the cross section. A clear difference in conductivity between the S2 layer and the middle lamella is apparent. No conclusion can be drawn on the S1 layer, as it is most likely influenced by topographical features (not shown). (b) Topography image on a transversal section. Although, overall, the image shows a good flatness, two grooves of the approximate size of the scanning probe (arrows) are apparent, which influence the conductivity contrast image. (c) Conductivity contrast image from the same scan. The grooves show an apparent higher conductivity. Apart from that, the S1 layer shows the greatest conductivity, followed by the middle lamella, and the S2 layer.

same conductivity, while a slight increase is visible along the S1 layer. Of special interest is the grainy structure of the S2, presumably caused by fibril bundles protruding from the sample due to the sample preparation with an ultramicrotome.

As shown in Figure 3, the variation in thermal conductivity between the anatomical directions is far larger than that between the cell wall layers in one anatomical direction, as becomes apparent when one standardized color scale is applied for the images from both planes. Here, the variations within one image become mostly negligible due to the strong contrast between the images. Especially for the transversal section, the only real variation still distinguishable is the increased conductivity caused by the vertical groove.

For the interpretation in the conductivity contrast images, the different effects responsible for the variations have to be considered. Variations within one image (Figure 2a and c) are caused by the anisotropy of the wood cell wall and show its different thermal behaviors on the nanoscale. In contrast, the strong differences in conductivity along the anatomical directions (Figure 3) could be caused by the penetration depth of the thermal energy as a "macroscopic" effect. Duvigneau et al. (2010) showed that the heat penetration depth for static measurements can be larger than 1 mm on poly(dimethyl siloxane). Though the data of the quoted literature are different from that in the present study (static instead of scanning, different material, higher temperatures), one can still presume that the heat penetration depth for our scans is at least some tens of micrometers. This means, especially for the transversal section, that the measurement is influenced by the subsurface cells and, therefore, by the cell arrangement.

However, it is still possible to compare the conductivity properties of the different cell wall layers within

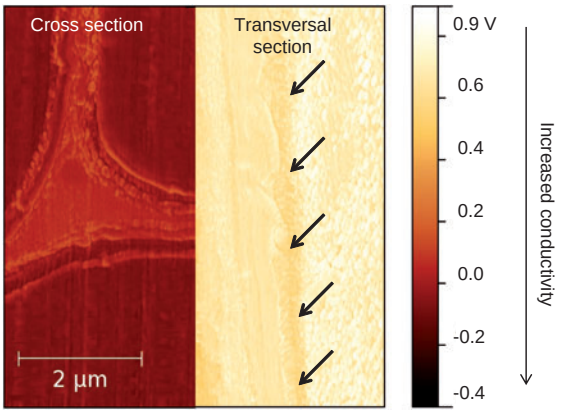

Figure 3 Comparison of the scans from Figure 2 with one color scale for both images. Although the variation in conductivity between the two directions is quite strong, the variations within one sample become mostly negligible. Arrows indicate the position of the topography groove causing a heightened conductivity.

the images. The variations between the S2 layer and the CML in Figure 2a and between the S1 layer, the S2 layer, and the CML in Figure 2c are real and caused by the deviating substructures of the cell wall. Eitelberger and Hofstetter (2011) presented a finite element model on the thermal transport mechanisms in wood. One of their main assumptions on the cell wall level was a high anisotropy of the thermal conductivity of crystalline cellulose, having a high conductivity parallel to the orientation of the cellulose chains (~1 W m^{-1} K^{-1}). Normal to the cellulose chains, they assumed a conductivity of ~0.25 W m^{-1} K^{-1}, which is slightly lower but of comparable size to the other cell wall materials. This assumption explains well the observed behavior.

In the cross section, the conductivity of the S2 layer is increased due to the nearly vertically oriented cellulose fibrils, while the lignin-rich CML has a decreased conductivity. On the transversal section, this difference vanishes as the fibrils in the S2 layer are nearly parallel to the surface. Here, the S1 layer shows an increased conductivity as could be expected from the fibrilar structure (Abe et al. 1991) and based on the above-mentioned assumption.

Conclusion

The thermal conductivity of the individual layers in the wood cell wall measured in the anatomical directions by SThM is different. Thus, the considerable macroscopic thermal anisotropy of wood can also be observed at the cell wall level. Probably, the orientation of the cellulose microfibrils strongly affects the thermal conductivity, with the highest conductivity along the microfibrils. The lignin-rich compound middle lamellae including the cell corners have clearly reduced conductivities compared to the S2. The present work demonstrates the potential of SThM without answering all open questions with this regard and would like to encourage further investigations in this field.

Received March 27, 2012; accepted August 9, 2012; previously published online xx

References

Abe, H., Ohtani, J., Fukazawa, K. (1991) FE-SEM observations on the microfibrillar orientation in the secondary wall of tracheids. IAWA Bull. 12:431–438.

Bader, T.K., Hofstetter, K., Alfredsen, G., Bollmus, S. (2012) Changes in microstructure and stiffness of Scots pine (*Pinus sylvestris* L) sapwood degraded by Gloeophyllum trabeum and Trametes versicolor – Part II: Anisotropic stiffness properties. Holzforschung 66:199–206.

Bastidas, J.C., Venditti, R., Pawlak, J., Gilbert, R., Zauscher, S., Kadla, J.F. (2005) Chemical force microscopy of cellulosic fibers. Carbohydr. Polym. 62:369–378.

Blanco, C., Appleyeard, S.P., Rand, B. (2002) Study of carbon fibres and carbon-carbon composites by scanning thermal microscopy. J. Microsc. 205:21–32.

Clauß, S., Gabriel, J., Karbach, A., Matner, M., Niemz, P. (2011) Influence of the adhesive formulation on the mechanical properties and bonding performance of polyurethane prepolymers. Holzforschung 65:835–844.

Duvigneau, J., Schönherr, H., Vancso, G.J. (2010) Nanoscale thermal AFM of polymers: transient heat flow effects. ACS Nano 4:6932–6940.

Eitelberger, J., Hofstetter, K. (2011) Prediction of transport properties of wood below the fiber saturation point – A multiscale homogenization approach and its experimental validation. Part I: Thermal conductivity. Compos. Sci. Technol. 71:134–144.

Fahlén, J., Salmén, L. (2005) Pore and matrix distribution in the fiber wall revealed by atomic force microscopy and image analysis. Biomacromolecules 6:433–438.

Fiege, G.B.M., Feige, V., Phang, J.C.H., Maywald, M., Görlich, S., Balk, L.J. (1998) Failure analysis of integrated devices by scanning thermal microscopy (SThM). Microelectron. Reliab. 38:957–961.

Follrich, J., Stöckel, F., Konnerth, J. (2010) Macro- and micromechanical characterization of wood-adhesive bonds exposed to alternating climate conditions. Holzforschung 64:705–711.

Hofstetter, K., Gamstedt, E.K. (2009) Hierarchical modelling of microstructural effects on mechanical properties of wood. A review COST Action E35 2004–2008: Wood machining – micromechanics and fracture. Holzforschung 63: 130–138.

Jäger, A., Hofstetter, K., Buksnowitz, C., Gindl-Altmutter, W., Konnerth, J. (2011) Identification of stiffness tensor components of wood cell walls by means of nanoindentation. Composites Part A 42:2101–2109.

Konnerth, J., Harper, D., Lee, S.H., Rials, T.G., Gindl, W. (2008) Adhesive penetration of wood cell walls investigated by scanning thermal microscopy (SThM). Holzforschung 62:91–98.

Lee, S.-H., Wang, S., Endo, T., Kim, N.-H. (2009) Visualization of interfacial zones in lyocell fiber-reinforced polypropylene composite by AFM contrast imaging based on phase and thermal conductivity measurements. Holzforschung 63: 240–247.

Lehringer, C., Koch, G., Adusumalli, R.-B., Mook, W.M., Richter, K., Militz, H. (2011) Effect of Physisporinus vitreus on wood properties of Norway spruce. Part 1: Aspects of delignification and surface hardness. Holzforschung 65:711–719.

Majumdar, A. (1999) Scanning thermal microscopy. Annu. Rev. Mater. Sci. 29:505–585.

Shi, L., Kwon, O., Miner, A.C., Majumdar, A. (2001) Design and batch fabrication of probes for sub-100 nm scanning thermal microscopy. J. MEMS 10:370–378.

Taguchi, A., Murata, K., Nakamura, M., Nakano, T. (2011) Scale effect in the anisotropic deformation change of tracheid cells during water adsorption. Holzforschung 65:253–256.

Wagner, R., Moon, R., Pratt, J., Shaw, G., Raman, A. (2011) Uncertainty quantification in nanomechanical measurements using the atomic force microscope. Nanotechnology 22:455703.

Wimmer, R., Lucas, B.N., Tsui, T.Y., Oliver, W.C. (1997) Longitudinal hardness and Young's modulus of spruce tracheid secondary walls using nanoindentation technique. Wood Sci. Technol. 31:131–141.

Yu, Y., Tian, G., Wang, H., Fei, B., Wang, G. (2011) Mechanical characterization of single bamboo fibers with nano-indentation and microtensile technique. Holzforschung 65: 113–119.

Curriculum Vitae

Education and Scientific Career

2012	COST-action training class on measurement of modulus of elasticity of wood in Montpellier, France
since 2011	PhD at BOKU Vienna
2010	internship as laboratory assistant at BOKU Vienna
2010	master thesis "Cross-Sectional Nanoidentification as Means of Adhesion Characterisation at the Wood-Adhesive Bond Line"
2008	exchange term at University of Swansea, Wales
2005-2010	studying physics at University of Vienna
2004	graduated high school at BG7BRG St. Veit/Glan

Main Research Fields

Micromechanical properties of natural fibres and natural fibre composite materials

Micro- and nano-characterisation methodology for natural fibre materials

Adhesion and adhesives characterisation

List of Publications

[1] Veigel S., Müller U., Keckes J., Obersriebnig M., Gindl-Altmutter W. (2011): Cellulose nanofibrils as filler for adhesives: effect on specific fracture energy of solid wood-adhesive bonds. CELLULOSE. 2011; 18 (5): 1227-1237

[2] Obersriebnig M., Veigel S., Gindl-Altmutter W., Konnerth J. (2012): Determination of adhesive energy at the wood cell-wall/UF interface by nanoindentation (NI). HOLZFORSCHUNG. 2012; 66 (6): 781-787

[3] Vay O., Obersriebnig M., Müller U., Konnerth J., Gindl-Altmutter W. (2013) Studying thermal conductivity of wood at cell wall level by scanning thermal microscopy (SThM). HOLZFORSCHUNG. 2013; 67 (2): 155-159

[4] Obersriebnig M., Konnerth J., Gindl-Altmutter W. (2013): Evaluating fundamental position-dependent differences in wood cell wall adhesion using nanoindentation. INT J ADHES ADHES. 2013; 40: 129-134

[5] Hauptmann M., Müller U., Obersriebnig M., Gindl-Altmutter W., Beck A., Hansmann C. (2013): The optical appearance of wood related to nanoscale surface roughness. BIORESOURCES. 2013; 3:4038-4045

[6] Ammann S., Obersriebnig M., Konnerth J., Gindl-Altmutter W., Niemz

P. (2013) Comparative adhesion analysis at glue joints in European beech and Norway spruce wood by means of nanoindentation. INT. J ADH ADH. 2014; 50: 45-49

[7] Guerriero G., Silvestrini L., Obersriebnig M., Salerno M., Pum D., Strauss, J. (2013) Sensitivity of Aspergillus nidulans to the cellulose synthase inhibitor dichlobenil: Insights from wall-related genes' expression and ultrastructural hyphal morphologies. PLoS ONE. 2013; 8 (11): Article number e80038

[8] Veigel S., Grüll G., Pinkl S., Obersriebnig M., Müller U., Gindl-Altmutter W. (2014) Improving the mechanical resistance of waterborne wood coatings by adding cellulose nanofibres. REACT FUNCT POLYM. (in print)

[9] Frybort S., Obersriebnig M., Müller U., Gindl-Altmutter W., Konnerth J. (2014) Variability in surface polarity of wood by means of AFM adhesion force mapping. COLLOID SURFACE A. 2013, 457 (1), 82-87